R E M A R K S

Claim 17 was objected to for the reason stated at the top of page 3 of the Office Action. Such reason was that claim 17 should have been preceded by the status identifier "withdrawn." The listing of claims submitted hereinabove sets forth the status identifier for claim 17 as "withdrawn."

Withdrawal of the objection to claim 17 is respectfully requested.

The present claim 3 is directed to a non-aqueous electrolyte for a lithium secondary battery to be used in combination with a positive electrode and a negative electrode capable of storing and releasing litium, which comprises a non-aqueous solvent and a lithium salt dissolved therein,

wherein the non-aqueous solvent comprises:

(a) at least one phosphate selected from the group consisting of (a1) a chain state phosphate and (a2) a cyclic phosphate;

(b1) a cyclic carboxylate;

(c1) a vinylene carbonate compound and

(c2) a vinylethylene carbonate compound.

The advantageous results afforded by the present claims are described on page 1, lines 28 to 35 of the present specification as follows.

The non-aqueous electrolyte containing a phosphate as recited in the present claims has excellent flame retardancy (self-extinguishing property) or nonflammability (having no flash point) and high conductivity, as well as electrochemical stability, so that it is possible to ensure safety of a lithium secondary battery. In addition, a secondary battery using the non-aqueous electrolyte, as recited in the present claims, exhibits excellent battery charge-discharge characteristics.

A phosphate is inferior in redox resistance to a conventionally used solvent and has a serious problem in that it lowers the charge-discharge characteristics of a battery as described on page 3, lines 16 to 26 of the present specification. Applicants' present claims serve to solve such problem.

Claims 3, 4, 9 to 11, 13 to 15, 18 and 19 were rejected under 35 USC 103 as being unpatentable over Tan et al. (JP 11-260401) in view of Yoshimura et al. (JP 4-087156) for the reasons set forth on pages 4 to 5 of the April 26, 2007 Office Action.

15

It was admitted in the April 26, 2007 Office Action that Tan et al. do not explicitly teach a vinylethylene carbonate compound.

Claims 20 to 27 were rejected under 35 USC 103 as being unpatentable over Tan et al. in view of Yoshimura et al. and further in view of Sonobe et al. (USP 5,527,643) and Kameda et al. (USP 6,632,569) for the reasons indicated on page 5, lines 4 to 11 of the April 26, 2007 Office Action.

It was admitted in the July 12, 2006 Office Action that Tan et al. do not explicitly teach a graphite carbonaceous material having a first plane spacing d_{002} value, or a second carbonaceous material having a second plane spacing d_{002} value.

Claims 28 to 30 were rejected under 35 USC 103 as being unpatentable over Tan et al. in view of Sonobe et al. and Kameda et al. and further in view of Watanabe et al. (USP 6,682,856) for the reasons set forth in the last three paragraphs on page 5 of the April 26, 2007 Office Action.

It was admitted in the July 12, 2006 Office Action that Tan et al. do not explicitly teach the claimed surface area or particle diameter for the carbonaceous material or a metal

selected from Sn, Si and Al.

Tan et al. (JP 11-260401) disclose the following:

"[Claim 1] Nonaqueous electrolyte characterized by consisting of a non-aqueous solvent containing the vinylene carbonate derivative expressed with the following general formula [I], and a phosphoric acid ester compound, and an electrolyte.

$$R^1 - C = C - R^2$$

[I]
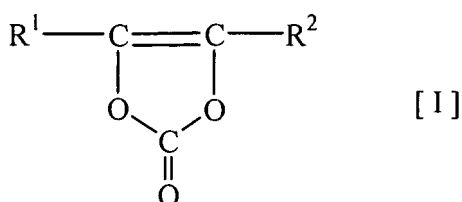
(Among a formula, even if R^1 and R^2 are mutually the same, they may differ from each other, and they show a hydrogen atom or the alkyl group of carbon numbers 1-3.)"

One of the most important characteristic features of applicants' present claim 3 resides in using (a) at least one phosphate selected from the group consisting of (a1) a chain state phosphate and (a2) a cyclic phosphate; and (b1) a cyclic carboxylate; in combination with both of (c1) a vinylene carbonate compound and (c2) a vinylethylene carbonate compound simultaneously.

Tan et al. do not teach or suggest using (c2) a vinylethylene carbonate compound as recited in applicants' present claim 3.

17

In applicants' present claims, by using vinylene carbonate (hereinafter referred to as "VC") and vinylethylene carbonate (hereinafter referred to as "VEC") in combination as components of the electrolyte, the problems involved in an electrolyte containing a phosphate were shown to be solved in the DECLARATION UNDER 37 CFR 1.132 of Yasuyuki SHIGEMATSU dated October 5, 2006. The above fact deeply relates to a reductive decomposition potential of a phosphate and the film-forming potentials of VC and VEC as discussed below.

According to evaluations by the present inventors after filing the present application, a reductive decomposition potential of trimethyl phosphate (hereinafter referred to as "TMP") can be estimated to be about 1.4V with a Li/Li+ standard. On the other hand, VC forms a good film on a negative electrode, which film inhibits a reductive decomposition at 0.8 to 1.3V (see the enclosed copy of Journal of Electrochemical Society, 151, A1659-A1669 (2004), specifically on page A1660, right column, line 4 from the bottom to page A1662, left column, line 7 from the bottom).

The above means that in an electrolyte containing TMP and VC like Tan et al. (JP 11-260401), the charging proceeds to reach a potential of a negative electrode of 1.4V, and a reductive decomposition of TMP proceeds before formation of a film of VC. That is, in an electrolyte containing TMP and VC, an effect of VC is small, and no effect can be obtained in some cases. On the other hand, VEC has been known to have a film-forming property, as also with respect of VC; and a film-forming potential of VEC is nobler than that of VC. Moreover, a film-forming reaction of VEC starts from about 1.4V (or 1.35V), which is substantially the same as the reductive decomposition potential (see the enclosed copy of <u>Electrochemistry Communications</u>, 6, 126-131, (2004), specifically on page 127, right column, line 7 starting from "3. Results and discussion" to page 128, left column, line 4 from the bottom.

Accordingly, VEC and VC are clearly different from each other, and by carrying out a reductive decomposition of TMP simultaneously with a film formation of VEC, the reductive decomposition of TMP can be controlled. However, the film formed by VEC is not as good as that formed by VC, and when it is used

19

as an additive of an electrolyte, its battery characteristics are not sufficient.

Thus, in applicants' present claims, by co-presenting VC in a non-aqueous electrolyte with VEC, more practical battery characteristics, can be obtained. That is, an electrolyte containing TMP in which reductive decomposition is stopped due to the film formation of VEC, is expected to carry out a film formation reaction by VC. The film formed by VC has better qualities for a lithium secondary battery than the film formed by VEC and improves battery characteristics. As a result, the battery characteristics of a battery containing both VC and VEC are more improved than a battery containing either one of VC or VEC, alone, and the former battery can provide a practical use.

As can be clearly seen from the above explanation, in Tan et al. (JP 11-260401), which uses VC alone, the battery characteristics, as accomplished in applicants' present claims, cannot be attained. Morevoer, in applcants' present claims, two kinds of solvents, both of which have film-forming action, are not simply mixed in an electrolyte. When a phosphate is used as a solvent for an electrolyte, and yet is contained in a higher

concentration for the purpose of improving flame retardency,

battery characteristics can be synergistically heightened by co-

presenting both VC and VEC having the above-mentioned mechanisms.

Moreover, according to the mechanisms as discussed above, it

would be drastically surprising to one of ordinary skill in the

art that battery characteristics (initial efficiency) could be

synergistically heightened to be 6% or more. In this regard, see

the Comparative example 1 of Example 34, which employs only VC,

as shown in Table 5 on page 4 of the previously submitted

DECLARATION UNDER 37 CFR 1.132 of Yasuyuki SHIGEMATSU dated

October 5, 2006, which was not charged or discharged, as shown in

Table 6 on page 5 of the October 5, 2006 Yasuyuki SHIGEMATSU

DECLARATION. However, due to the co-presence of VC and VEC,

Example 34 showed a high charge-discharge efficiency (see Table 6

of the October 6, 2006 Yasuyuki SHIGEMATSU DECLARATION). For

example, the attached copy of Electrochimica Acta, 52, 6006-6011,

(2007), shows that by washing, heat-treating and coating graphite

(negative electrode active substance), the initial charge-

discharge efficiency was improved 6 to 12%, as compared with

21

untreated graphite, as shown in Table 1 on page 6008.   Such an increment of the initial charge-discharge efficiency is described as having been greatly improved in the column of "4. Conclusions" on page 6010, right column thereof.

In the cited references of Sonobe et al., Kameda et al., and Watanabe et al., only various kinds of negative electrodes are disclosed, but there is no teaching or suggestion to use the specific electrolyte as defined in applicants' present claim 3. These references also do not teach or suggest the advantageous results afforded by applicants' claims.
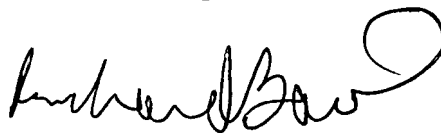
In view of the above, withdrawal of each of the obviousness rejections is respectfully requested.

Reconsideration is requested.   Allowance is solicited.

If the Examiner has any comments, questions, objections or recommendations, the Examiner is invited to telephone the undersigned at the telephone number given below for prompt action.

Respectfully submitted,

Frishauf, Holtz, Goodman
& Chick, P.C.
220 Fifth Ave., 16th Floor
New York, NY 10001-7708
Tel. No. (212) 319-4900   Richard S. Barth, Reg. No. 28,180
Fax No.: (212) 319-5101
E-Mail Address: BARTH@FHGC-LAW.COM
RSB/ddf

Enclosures: (1) PETITION FOR EXTENSION OF TIME

             (2) a copy of Journal of Eelctrochemical Society,
                  151, A1659-A1669, (2004)

             (3) a copy of Electrochemistry Communications,
                  6, 126-131, (2004)

             (4) a copy of Electrochimica Acta, 52,
                  6006-6011, (2007)

Analysis of Vinylene Carbonate Derived SEI Layers on Graphite Anode

Hitoshi Ota,[a],[*],[z] Yuuichi Sakata,[a] Atsuyoshi Inoue,[a] and Shoji Yamaguchi[b],[*]

[a]Mitsubishi Chemical Group Science and Technology Research Center, Inc., 8-3-1 Chu-o Ami, Inashiki, Ibaraki 300-0332, Japan
[b]Mitsubishi Chemical Corporation, 33-8 Shiba 5-chome, Minato-ku, Tokyo 108-0014, Japan

The solid electrolyte interface (SEI) formation on composite graphite and highly oriented pyrolytic graphite in a vinylene carbonate (VC)-containing electrolyte was analyzed using evolved gas analysis, Fourier transform infrared analysis, two-dimensional nuclear magnetic resonance, X-ray photoelectron spectroscopy, time of flight-secondary-ion mass spectrometry, and scanning electron microscopy. We found that the SEI layers derived from VC-containing electrolytes consist of polymer species such as poly (vinylene carbonate) (poly(VC)), an oligomer of VC, a ring-opening polymer of VC, and polyacetylene. Moreover, lithium vinylene dicarbonate, $(CHOCO_2Li)_2$, lithium divinylene dicarbonate, $(CH=CHOCO_2Li)_2$, lithium divinylene dialkoxide, $(CH=CHOLi)_2$, and lithium carboxylate, $RCOOLi$, were formed on graphite as VC reduction products. The presence of VC in the ethylene carbonate (EC)-based electrolyte caused a decrease in the reductive gases of the EC dimethyl carbonate solvent such as C_2H_4, CH_4, and CO. The VC-derived SEI layer was formed at a potential more positive than 1.0 V vs. Li/Li^+. Effective SEI formation by reduction of VC progresses before that of EC. The thermal decomposition temperature of the SEI layer derived from VC shifted to a higher temperature compared to that derived from the VC-free electrolytes. We concluded that the thermal stability of the VC-derived SEI layer has a close relation to high-temperature storage characteristics at elevated temperatures.
© 2004 The Electrochemical Society. [DOI: 10.1149/1.1785795] All rights reserved.

Rechargeable lithium batteries using a carbon anode are presently one of the major power sources for portable electronic devices because of their high voltage and high energy density. Most research performed to advance the lithium-ion battery has concentrated on improving the aspects of battery performance such as cycling characteristics, high-temperature storage, and rate characteristics. Numerous studies have been done on developing new electrolytes for lithium batteries with high ionic conductivity and good chemical and electrochemical stabilities.[1-5] In addition, some inorganic compounds[6-10] and organic compounds such as unsaturated carbon bond-containing components,[11-15] sulfur-containing components,[16-19] halogen-containing components,[20-24] and other components[25-27] have been proposed electrolyte as additives for lithium-ion batteries. It is considered that these additives improve the properties of the solid electrolyte interface (SEI) layer formed on the graphite anode.

Vinylene carbonate (VC) has been proposed as an electrolyte additive to improve battery performance.[11] The use of VC as an additive in a propylene carbonate (PC)-based electrolyte can suppress gas evolution.[11] The PC-based electrolytes are more favorable from the viewpoints of their low-temperature characteristics and flash point of the solvent compared to ethylene carbonate (EC)-based electrolytes. However, commercial lithium batteries have used EC-based solvents and not PC-based solvents, in which the exfoliation of graphite occurs. The presence of VC as an additive can prevent the co-intercalation of PC. The addition of VC to the EC-based electrolyte is effective as well as in the PC-based electrolyte.[28-30] The cycling performance and high-temperature storage are improved by adding VC to the EC-based electrolyte. VC has been recognized as an effective additive for the electrolyte when using a graphite anode.

Several studies have been done on the VC-derived SEI layers.[29-32] Aurbach et al. reported that the presence of VC in EC + DMC (1:1) containing LiAsF₆ led to polymerization on the lithiated graphite surface.[29] The results of Fourier transform infrared (FTIR) spectroscopy indicated that the reduction of VC forms polymeric chains (containing -OCO₂Li groups) by reactions of the double bonds. However, a more detailed polymer structure could not be described. The SEI formation due to the presence of VC in the electrolyte was investigated using in situ atomic force microscopy.[32]

The morphological change of the highly oriented pyrolytic graphite (HOPG) basal plane in $LiClO_4$/PC + VC 3 wt % was observed at a potential around 1.35 V, and particle-like precipitates were formed by the reductive decomposition of VC before the reduction of PC.[32] The VC-derived SEI layer on the HOPG consists of a thin film compared to the SEI layer in the VC-free electrolyte.[30] The electroreductive decomposition of PC + VC and EC + VC has been investigated using the density functional theory (DFT) calculation. VC is initially reduced to a more stable intermediate than the reduction of EC and PC. The reduced VC decomposes to form a radical anion via a barrier of about 20 kcal/mol, and the subsequent radical anion termination generates the proper products dominated by unsaturated lithium alkyl dicarbonates.[33,34]

Although some attempts have been made to analyze the VC-derived SEI layer, the detailed structure is unknown. The purpose of this study is to clarify the structure of the VC-derived SEI layer formed on the graphite anode by cyclic voltammetry, NMR, FTIR spectroscopy, time of flight-secondary-ion mass spectrometry (TOF-SIMS), X-ray photoelectron spectroscopy (XPS), and scanning electron microscopy (SEM). FTIR and XPS have been used for the structural analysis of the SEI layer. Very few attempts have been to analyze the SEI layer by NMR spectroscopy, which has been established as a powerful, highly useful technique for structural elucidation.[35] Recently, the surface structure of the SEI layer has been analyzed using TOF-SIMS, which is more convenient for obtaining the structure of the polymer.[36] The evolved gas species during initial charging were measured to clarify the mechanism of the SEI formation. To evaluate the thermal stability of electrodes, the open-circuit voltages (OCV) of a three-electrode cell ($LiCoO_2$/graphite ion cell), using lithium as a reference electrode, were measured at 60°C.

We investigated the thermal stability of the VC-derived SEI layer by temperature programmed desorption (or decomposition)-mass spectrometry (TPD-MS). TPD-MS was used to understand the stability of the VC-derived SEI layer at elevated temperatures.

Experimental

Sample preparation.—A graphite powder sample [Mitsubishi Power Graphite (MPG), Mitsubishi Chemical Corporation] and HOPG blocks (Advanced Ceramics) were used as the anode materials. The composite electrode was prepared from a mixture of 92 wt % graphite powder with 8 wt % polyvinylidene fluoride (PVdF) on copper foil. Lithium was used as the counter electrode. The electro-

lyte was 1 mol dm^{-3} lithium hexafluorophosphate ($LiPF_6$) in a 1:1 by volume EC + dimethyl carbonate (DMC) mixture (Sol-Rite, Mitsubishi Chemical Corporation). The concentration of VC (Mitsubishi Chemical Corporation) was 2 wt % of the electrolyte. Moreover, 1 mol dm^{-3} $LiPF_6$/VC was used as an electrolyte to analyze the SEI formation of pure VC. The electrodes were separated by a polyethylene separator. The charge (lithium intercalation) and discharge (lithium deintercalation) were conducted in a two-electrode half-cell. Cells were assembled in an argon-filled glove box. The charge-discharge measurements were performed in the galvanostatic mode using charge-discharge equipment (Nagano, BTS-2004w) at 25°C in a constant temperature oven maintained within ±0.5°C. The Li/composite graphite and Li/HOPG half-cells were charged to a potential of 0 V (vs. Li/Li$^+$) at current densities of 0.2 mA/cm^2 (composite graphite) and 0.01 mA/cm^2 (HOPG). The Li-doped graphite was discharged at current densities of 0.4 mA/cm^2 (composite graphite) and 0.01 mA/cm^2 (HOPG) to 1.5 V (vs. Li/Li$^+$). The cell was dismantled in the argon-filled glove box. The analytical samples were transported to instruments using inactive transfer vessels.

Cyclic voltammetry.—A three-electrode electrochemical cell was employed for the cyclic voltammetry measurements. The working electrode was composite graphite, and the reference and counter electrodes were lithium metal. Cyclic voltammetry was performed at 25°C at a sweep rate of 0.2 mV/s between 2.5 and 0 V vs. Li/Li$^+$.

Evolved gas analysis.—The charge (Li intercalation) operation was carried out using a assembly-cell type (stainless steel) without breaking the seal. The evolved gas in the cell was analyzed by gas chromatography (GC). Separation of the degradation products in the evolved gases was obtained using a plot-Q column and a molecular sieve column. The GC column was programmed at a constant temperature of 70°C.

Microscopic observations.—After the charge-discharge test, the HOPG anode was removed from the coin cell and rinsed with highly purified dimethoxyethane (F-DME, battery grade, Mitsubishi Chemical Corporation) to remove electrolyte. The water content in DME was detected to be <5 ppm. After drying under vacuum for 30 min, the HOPG anode was moved for surface observation with a transfer vessel. The morphologies of the SEI layer were observed using SEM (JEOL, JEM-6300F).

NMR spectroscopy.—Organic SEI layers in the state of lithium deintercalation on the composite graphite in 1 mol dm^{-3} $LiPF_6$/VC were dissolved with dimethyl sulfoxide (DMSO)-d_6 in an argon-filled box. We used a solution of the dissolved SEI layer with DMSO-d6 for the NMR measurements. All NMR spectra were obtained using an NMR spectrometer (JEOL JNM-GSX400) operating at 400 MHz for the ^{1}H nucleus and 100 MHz for the ^{13}C nucleus. All spectra were recorded at room temperature, and DMSO was used as the internal standard. The conditions for the ^{1}H-NMR were 45° pulse angle, 7.3 s delay between pluses, 20.0 kHz spectral width, and 64 scans. The conditions for the ^{13}C-NMR were a 45° pulse angle, 1.8 s delay between pluses, 27 kHz spectral width, and 27,000 scans. The ^{1}H-detected multiple quantum coherence (HMQC) spectrum was acquired in the magnitude mode using 64 scans for each 256 $t1$ increments, a 1.2 s recovery delay, spectral widths in f1 and f2 of 4.5 and 22.0 kHz, respectively, an evolution delay (1/(2J)) of 3.8 ms, an acquisition time of 0.224 s, 24.0 i s 90° ^{1}H pulses, and 9.2 μs 90° ^{13}C pulses. The ^{1}H-detected multiple-bond heteronuclear multiple quantum coherence (HMBC) spectrum was acquired in the magnitude mode using 160 scans for f1 and f2 of 512 t1 and 256 t1 increments, 1.5 s recovery delay, spectral widths in f1 and f2 of 4.6 and 20.0 kHz, an evolution delay (1/(2J)) of 3.8 ms, an acquisition time of 0.224 s, 24.0 μs 90° ^{1}H pulses, and 9.2 μs 90° ^{13}C pulses. The proton-proton correlation spectroscopy (^{1}H-^{1}H COSY) was acquired in the magnitude mode using 64 scans for f1 and f2 of 512 t1

and 256 t1 increments, a 1.3 s recovery delay, spectral widths in f1 and f2 of 3.7 kHz, an acquisition time of 0.273 s, and 24.0 μs 90° ^{1}H pulses.

XPS.—XPS (ULVAC-PHI5700ci) was used to obtain information about the elementary chemical state and depth profile distribution for the SEI layer on the graphite anode at 25°C. The electrolyte containing the SEI layer was removed using highly purified DME. After drying under vacuum for 30 min, the graphite anode was moved for surface analysis by using a transfer vessel. Monochromatic Al K radiation (1486.6 eV), operated at a power of 350 W (14 kV), was applied as the X-ray source. The emission angle, i.e., the angle between the sample normal and the analyzer entrance, was about 65°, to enhance the surface sensitivity. Samples for the XPS measurements were made by stopping at each potential of the SEI formation during the initial charging (Li intercalation) process. The potentials were 1.0, 0.6, 0.25 (LiC_{72}), 0.05 (LiC_{12}), and 0 V (LiC_6) vs. Li/Li$^+$. All XPS measurements were taken in the state of lithium deintercalation. Sputtering of the sample surface was performed with an argon ion gun under an accelerating voltage of 3 kV. All the samples were measured after 0, 1, 5, 15, 45, 90, and 150 min of Ar$^+$ ion sputtering. The sputtering time is estimated to be 2 nm/min for SiO_2/Si film.

FTIR.—The organic components of the SEI layers in the state of lithium deintercalation on the composite graphite at 25°C were characterized by an FTIR spectrometer (Nicolet Magna500) equipped with a triglycine sulfate detector. The sample for FTIR study was moved using an inactive vessel. The electrolyte containing the SEI layer was removed by highly purified DME. The measurement was carried out using the attenuated total reflection (ATR) method. Ge was used for the ATR crystals. Spectra were recorded with a resolution of 4 cm^{-1}; and 32 interferogram scans were averaged, providing spectra from 650 to 4000 cm^{-1}.

TOF-SIMS.—TOF-SIMS was used to provide structural information on the surface about the SEI layer in the state of lithium deintercalation on the HOPG anode at 25°C. TOF-SIMS measurements were performed with a TRIFT II (Physical Electronics) using a ^{69}Ga primary ion beam (15 keV impact energy) operating at a 600 pA beam current. The analyzed area was 80 × 80 μm. The electrolyte containing the SEI layer on the HOPG anode was removed with highly purified DME.

Evaluation of thermal stability for batteries.—A three-electrode cell was used to evaluate the thermal stability of the electrodes. $LiCoO_2$ (Nippon Chemical Industry) was used as the cathode material, and graphite powder (MPG) was used as the anode material. A polyethylene separator separated the electrodes. Lithium was used as the reference. Lithium cobalt oxide electrodes were prepared by mixing 94 wt % $LiCoO_2$ with 3 wt % acetylene black and 3 wt % PVdF, and then coating the mixture on aluminum foil. The graphite electrode was prepared from a mixture of 92 wt % graphite powder with 8 wt % PVdF on copper foil. The three-electrode cells were assembled in an argon-filled glove box. The cells were charged and discharged between 4.2 and 3.0 at a constant current density of 0.6 mA/cm^2 (charged) and 1.5 mA/cm^2 (discharged) at 25°C. The three-electrode cells in fully discharged state [state of charge (SOC) 0%] were stored for 3 days at a constant temperature of 60°C. The OCV of the cells was monitored during high-temperature storage to analyze the thermal stability of the battery. The thermal stability of the SEI layer formed on the composite graphite was evaluated using TPD-MS (ANELVA AGS-7000). The analytical sample was transported using the argon-filled transfer vessel to prevent degeneration of the sample by air exposure.

Results and Discussion

Reductive decomposition of VC by cyclic voltammetry.—Cyclic voltammograms (CVs) of a composite graphite anode in the EC + DMC (1:1) electrolyte containing $LiPF_6$ exhibited a reductive
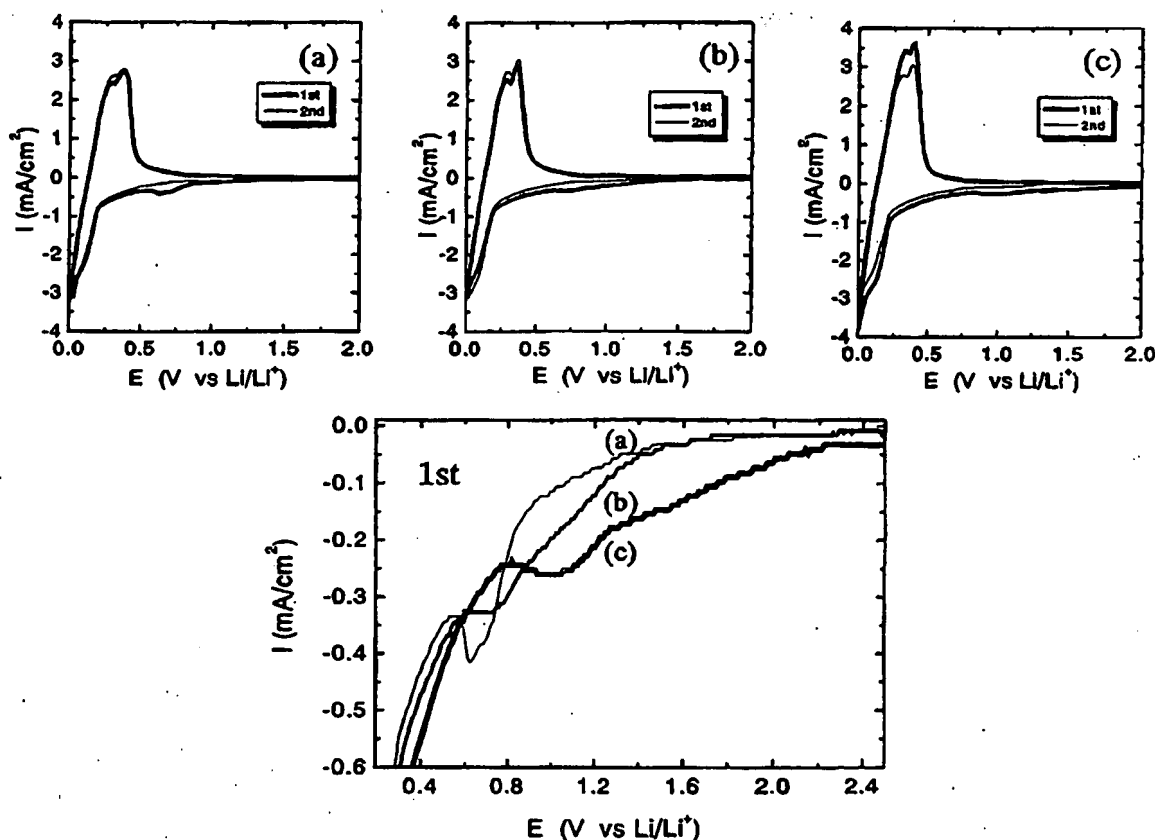
Figure 1. CVs of composite graphite anode in (a) 1 mol dm^{-3} LiPF$_6$/EC + DMC (1:1), (b) 1 mol dm^{-3} LiPF$_6$/EC + DMC (1:1) + 2 w/ % VC, and (c) 1 mol dm^{-3} LiPF$_6$/VC at 25°C. Sweep rate: 0.2 mV/s.

peak at 0.7 V (cathodic sweep) as shown in Fig. 1a and b. No reductive peak could be detected for the secondary CV. In the LiPF$_6$/EC electrolyte, the peak at 0.7 V can be observed due to the reduction of EC. By adding VC to the EC-based electrolyte, the reductive peak was observed at 0.8 V and decreased as shown in Fig. 1b. A reductive peak related to VC was detected at 1.1 V in the VC-containing electrolyte (Fig. 1b) and the LiPF$_6$/VC electrolyte (Fig. 1c). Moreover, a reductive current flowed from the potential of around 1.4 and 2.2 V in the VC-containing EC-DMC electrolyte and the LiPF$_6$/VC electrolyte, respectively. The effective SEI formation progresses by reduction of VC before that of EC. As a result, the reductive peak related to EC diminished because of the VC-derived SEI formation. The peak potential on adding VC shifted from 0.7 to 0.8 V vs. Li/Li$^+$. According to DFT calculations, the VC-reduction intermediate is that the ring opening occurs on the unreduced EC moiety instead of on the reduced VC, via an intramolecular electron-transfer transition state. The CV result showed that the reductive peak at 0.7 V related to EC was shifted to 0.8 V by adding VC. The presence of VC in the EC-based electrolyte may promote the ring opening of EC.

Figure 2 shows the dQ/dV curves of the first charging (Li intercalation) using the Li/graphite half-cell. The results of the dQ/dV curves corresponded to the CV results. The electrolyte with VC had a reductive peak at 1.1 V and a decreased peak related to EC at 0.8 V. Zhang *et al.* reported that the reduction of VC in tetrahydrofuran

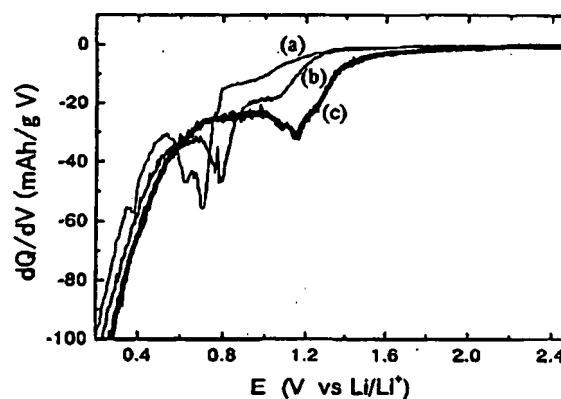**Figure 2.** The dQ/dV curves of composite graphite anode in (a) 1 mol dm^{-3} LiPF$_6$/EC + DMC (1:1), (b) 1 mol dm^{-3} LiPF$_6$/EC + DMC (1:1) +2 wt % VC, and (c) 1 mol dm^{-3} LiPF$_6$/VC at constant current of 0.16 mA/cm^2 at 25°C.
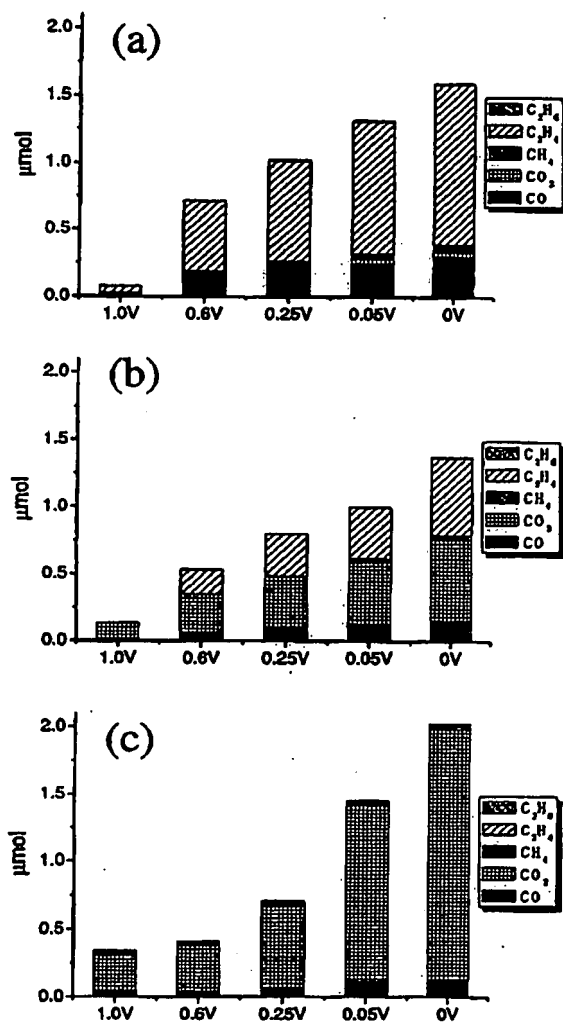
Figure 3. Evolved gas analysis during initial charge process (Li intercalation) in composite graphite anode/Li half-cell at 25°C. The electrolytes were (a) 1 mol dm^{-3} LiPF$_6$/EC + DMC (1:1), (b) 1 mol dm^{-3} LiPF$_6$/EC + DMC (1:1) + 2 wt % VC, and (c) 1 mol dm^{-3} LiPF$_6$/VC.
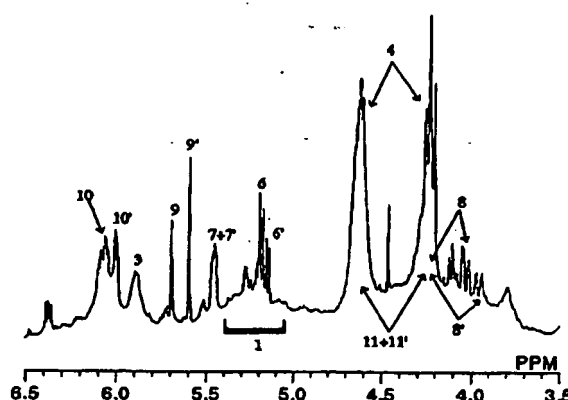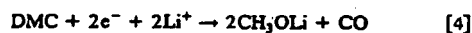

Figure 4. ^{1}H-NMR spectrum of dissolved solution with DMSO-d6 of SEI layer formed on composite graphite anode in 1 mol dm^{-3} LiPF$_6$/VC electrolyte.

$$2EC + 2e^- + 2Li^+ \rightarrow (CH_2OCO_2Li)_2 + C_2H_4 \quad [1]$$

$$EC + 2e^- + 2Li^+ \rightarrow (CH_2OLi)_2 + CO \quad [2]$$

$$DMC + e^- + Li^+ \rightarrow CH_3OCO_2Li + CH_3 \quad [3]$$

$$DMC + 2e^- + 2Li^+ \rightarrow 2CH_3OLi + CO \quad [4]$$

$$CH_3 + H \cdot \rightarrow CH_4 \quad [5]$$

The presence of VC in the EC-based electrolyte decreased the reductive gases of the EC-DMC electrolyte as C_2H_4, CH_4, and CO. Because no CH_4 can be seen in the only EC electrolyte, CH_4 mainly depends on the reduction of DMC. According to Reaction 3, DMC produces a CH_3 radical, which reacts with the H radical. The H radical could be mainly attributed to H_2O in the electrolyte and electrodes. We confirmed that a large quantity of hydrogen evolves after the first cycle in the Li/graphite half-cell when the water content in the electrolyte and graphite electrode is higher than the normal condition. Evolution of hydrogen mainly occurs from water reduction at the graphite electrode. CO_2 was detected at 1.0 V vs. Li/Li$^+$ and then increased with the intercalation of Li in the VC-containing electrolyte. Only the VC electrolyte produced a large amount of CO_2 and a little CO (Fig. 3c). We consider that CO_2 formation is due to the decarboxylation ($O=C—O^-$) of VC. In addition to CO_2 and CO, acetylene (C_2H_2) could be detected as the reductive decomposition gas of VC. However, detected acetylene in the battery reaction was very low. As discussed based on the results of the cyclic voltammetry, the VC-containing electrolyte underwent reductive decomposition at a potential more positive than at 1 V. The VC-containing electrolyte can suppress gas evolution of C_2H_4, CO, and CH_4 related to the reduction of the EC-DMC solvent. The result of the evolved gas has a significant connection with that of the CVs. The evolved gas results indicate that the VC additive works to suppress the SEI formation by EC.

Analysis of the VC derived SEI layer by NMR.—Figures 4-8 show the ^{1}H, ^{13}C, ^{1}H-^{1}H COSY, 2D ^{1}H-^{13}C HMQC, and 2D ^{1}H-^{13}C HMBC NMR spectra of the dissolved solution with DMSO of the SEI layer on the composite graphite anode in LiPF$_6$/VC. We assigned four components from the results of the NMR spectroscopy, as shown in Fig. 9. The assignments of the SEI compounds are summarized in Table 1. The assignments of the signals were decided by a combination of the following: (*i*) analysis of the proton-proton, proton-carbon in the 2D NMR spectra; (*ii*) comparison of the chemi-
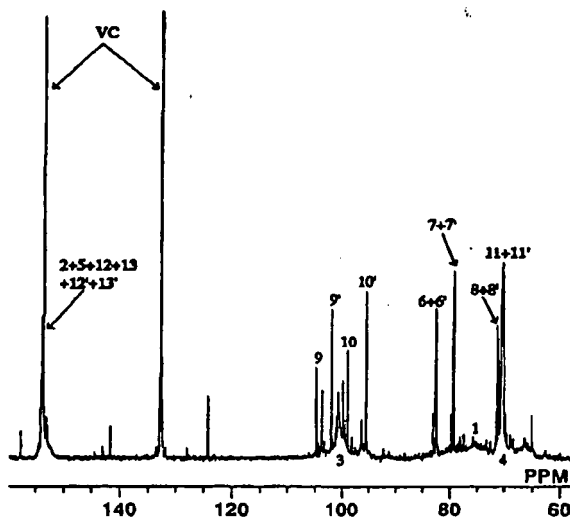
THF on a solution containing LiClO$_4$ with 1 vol % VC on Au electrode occurred at 1.4 V.[31] Jeong *et al.* reported that the reductive peak of VC in PC solution containing LiClO$_4$ with 3 wt % VC on the HOPG basal plane was observed at 1.3 V.[32] Although the peak potentials are different for the various electrolytes and anode, the reduction of VC occurs at a potential more positive than at 1 V (vs. Li/Li$^+$).

Evolved gas analysis after initial charge.—Figure 3 shows the evolved gas analysis during the first charging process (Li intercalation) of the composite graphite anode. Ethylene (C_2H_4), carbon monoxide (CO), and methane (CH_4) were detected in the EC-DMC (1:1) electrolyte. These gas species would be related to the formation of the SEI layer as in the following equation

Figure 5. ^{13}C-NMR spectrum of dissolved solution with DMSO-d6 of SEI layer formed on composite graphite anode in 1 mol dm^{-3} LiPF$_6$/VC electrolyte.
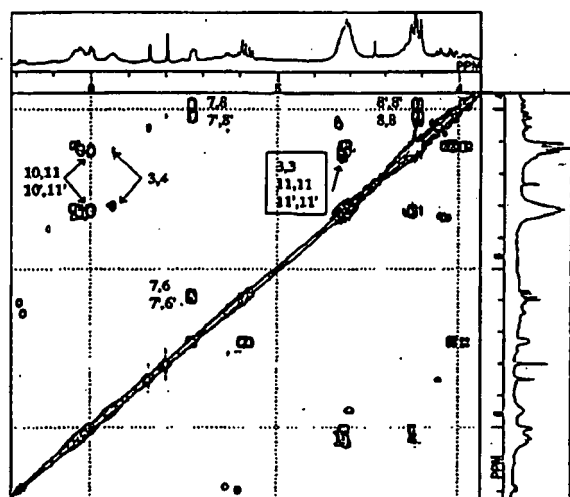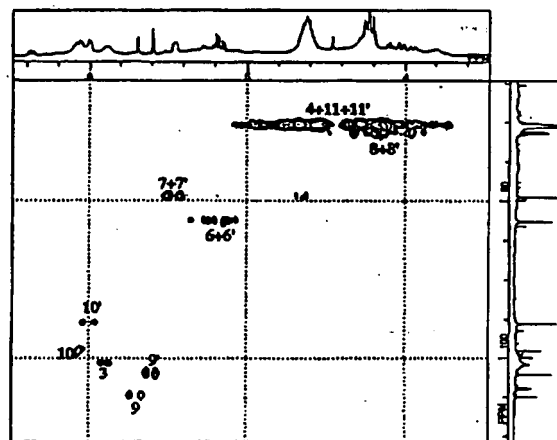

Figure 7. 2D ^{1}H-^{13}C HMQC spectrum of dissolved solution with DMSO-d6 of SEI layer formed on composite graphite anode in 1 mol dm^{-3} LiPF$_6$/VC electrolyte.

cal shifts of compound 1 with the synthetic compound [poly (VC)]; and (*iii*) comparison of the calculated ^{1}H and ^{13}C NMR chemical shifts.

Compound 1 was determined to be poly (VC) because the signals in the ^{1}H, ^{13}C-NMR spectra of poly (VC) corresponded to the signals of the dissolved solution of the SEI layer, as shown in Fig. 10. Generally, the polymer consistently provides a broad peak. Poly (VC) has a broad peak of the proton H-1 around 5.1-5.4 ppm and the carbons C-1 at 75.4 ppm and C-2 at 153.8 ppm. Poly(VC) was

slightly detected from the electrolyte after one cycle, as shown in Fig. 10b. This may be due to dissolution of SEI layer formed on the graphite.

The structure of compound 2 is shown in Fig. 9. The protons (H-4) at 4.22 and 4.56 ppm were directly attached to the carbon (C-4) at 70.3 ppm in the HMQC spectrum (Fig. 7). The protons have a correlation to the proton (H-3) at 5.89 ppm in the ^{1}H-^{1}H COSY spectrum (Fig. 6). Moreover, the proton (H-3) at 5.89 ppm was directly attached to the carbon (C-3) at 100.7 ppm in the HMQC spectrum. Based on this chemical shift, the signals are assigned to
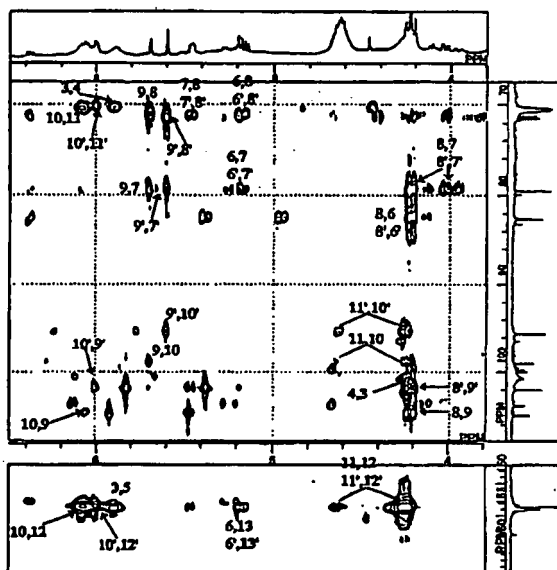

Figure 6. ^{1}H-^{1}H COSY spectrum of dissolved solution with DMSO-d6 of SEI layer formed on composite graphite anode in 1 mol dm^{-3} LiPF$_6$/VC electrolyte.

Figure 8. 2D ^{1}H-^{13}C HMBC spectrum of dissolved solution with DMSO-d6 of SEI layer formed on composite graphite anode in 1 mol dm^{-3} LiPF$_6$/VC electrolyte.

Compound 1   Compound 2   Compound 3
                                        Compound 4
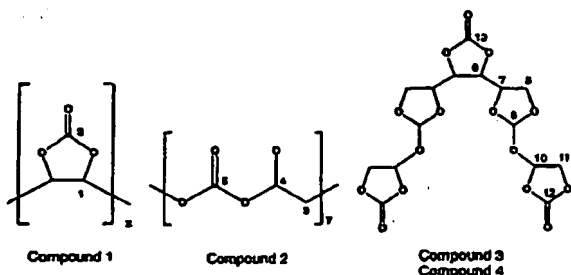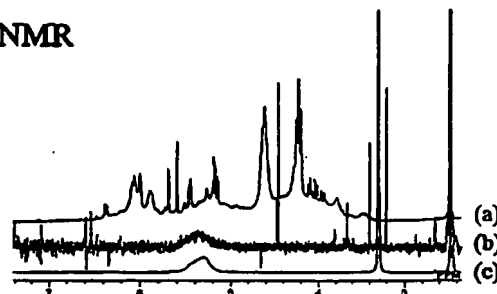
Figure 9. The structure of VC-derived SEI layer obtained from NMR spectroscopy.

the partial structure of O—C—O. The protons (H-4) at 4.22 and 4.56 ppm give a cross peak to the carbonate carbon (C-5) at 153.8 ppm in the HMBC spectrum (Fig. 8). Therefore, the protons (H-4) at 4.22 and 4.56 ppm and the carbons (C-3, C-4) at 100.7 and 70.4 ppm were assigned to compound 2. We estimate that compound 3 is a polymer component because the protons (H-3, H-4) and carbon (C-3, C-4) consist of broad peaks.

Compound 3 was determined as an oligomer component of VC. The integral ratio of H-6 (CH): H-7 (CH): H-8 (CH₂) was about 1:1:2 in the ¹H-NMR spectrum (Fig. 4). Based on the ¹H-¹H COSY spectrum (Fig. 6), the proton peak (H-7) at 5.45 ppm corresponded to the proton peaks (H-6, H-8) at 5.19 ppm and 4.03/4.25 ppm. In the HMQC spectrum (Fig. 7), the proton peaks (H-6, H-7) at 5.19 and 5.45 ppm were related to the carbon peaks at 82.6 and 79.4 ppm. The carbon chemical shift around 80 ppm suggests that the structure consists of a ring unit. The two protons (4.03 and 4.25 ppm) of H-8 produced a nonequivalence peak. The proton of H-9 at 5.7 ppm was related to the carbon of C-9 at 104.8 ppm (Fig. 7). In the HMBC spectrum (Fig. 8), the proton of H-9 gave cross peaks of the carbons of C-7 (79.4 ppm), C-8 (71.3 ppm), and C-10 (95.5 ppm). The carbon of C-10 (95.5 ppm) could be assigned the O—C—O unit from the chemical shift of the carbon. The ¹H-¹H COSY spectrum (Fig. 6) shows that the proton of H-10 is related to

Table I. ¹H and ¹³C NMR chemical shifts of dissolved solution with DMSO-d6 of SEI layer formed on composite graphite anode in 1 mol dm⁻³ LiPF₆/VC electroyte.

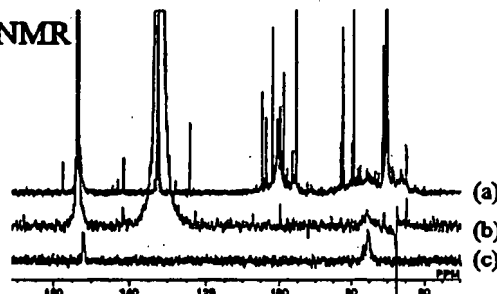|	Assignment	¹H chem. shift (ppm)	¹³C chem. shift (ppm)
Compound 1	1	75.40	5.3
	2	153.80	
Compound 2	3	100.70	5.9
	4	70.30	4.22, 4.56
	5	153.80	
Compound 3	6	82.60	5.2
	7	79.40	5.5
	8	71.30	4.03, 4.25
	9	104.80	5.7
	10	95.50	6.1
	11	70.60	4.25, 4.63
	12	153.60	
	13	153.60	
Compound 4	6'	82.50	5.2
	7'	79.40	5.5
	8'	71.10	3.96, 4.22
	9'	102.00	5.6
	10'	98.90	6.0
	11'	70.10	4.25, 4.63
	12'	153.60	
	13'	153.60	

¹H NMR

¹³C NMR

Figure 10. Comparison between (a) dissolved solution with DMSO-d6 of SEI layer on composite graphite anode in 1 mol dm⁻³ LiPF₆/VC electrolyte and (c) Poly (VC). Spectrum (b) is ¹³C NMR of electrolyte after the first lithium intercalation/deintercalation in LiPF₆/VC.

the proton of H-11. The protons of H-10 and H-11 give cross peaks of the carbonate carbon of C-12 (153.6 ppm) in the HMBC spectrum (Fig. 9). Moreover, the proton of H-6 is related to the carbonate carbon of C-13 (153.6 ppm). However, no H-6 proton relation can be observed to another bond except for C-7, C-8, and C13 in the ¹H-¹H COSY and the HMBC spectra. We believe that this compound consists of a symmetrical structure. Therefore, compound 3 can lead to the structure shown in Fig. 9. Compound 3 has some chiral carbon in the molecule. Based on the 2D-NMR spectroscopy, compound 4 has the same structure as compound 3. Compound 4 is an isomer because the ¹H and ¹³C chemical shifts of compound 4 can be detected close to that of compound 3.

Surface analysis of the VC derived SEI layer by XPS and SEM.— Figure 11 shows the C 1s and O 1s XPS spectra for the SEI layers formed on the composite graphite after the first lithium intercalation-deintercalation at 25°C. The SEI layer (Fig. 11a and b) formed on the graphite anode in the EC-based electrolyte shows peaks related to lithium alkyl carbonate at 291.1 eV (CO₃), 287.5 eV (CH₂O), and 285.8 eV (CH₂CH₂O) in the C 1s spectra and at 533.5 eV (C—O—C) and 532.5 eV (C=O) in the O 1s spectra. In addition to lithium alkyl carbonate, the VC-derived SEI layer (Fig. 11b) had peaks at 291.8 eV in the C 1s spectrum and at 534.4 eV in the O 1s spectrum. These binding energies of the VC derived SEI layer were higher than those of the lithium alkyl carbonate. The peaks would be assigned to poly (VC) as shown in Fig. 11c. The oxygen peak (C—O—C) related to polyethylenecarbonate (Fig. 11d, 11e) has a high binding energy in comparison with the alkyl carbonate. Moreover, the VC derived SEI layer can be seen as a carbon peak related to the ester (-COO) at 289 eV. Based on FTIR spectroscopy, as described in the next section, the VC derived SEI layer contains lithium carboxylate (-COOLi). The XPS results suggested the exhibited existence of the carboxylate from the top layer of the SEI in the VC-containing electrolyte. The intensity of the C 1s
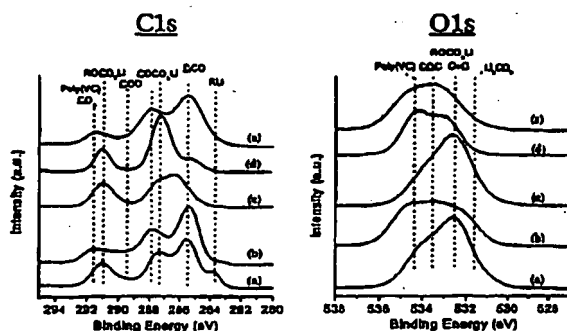
Figure 11. C 1s and O 1s XPS spectra for SEI layers formed on composite graphite in (a) 1 mol dm^{-3} LiPF$_6$/EC + DMC (1:1), (b) 1 mol dm^{-3} LiPF$_6$/EC + DMC (1:1) + 2 w/ % VC at 25°C. Spectra (c), (d), and (e) were C 1s and O 1s XPS spectra of CH$_3$CH$_2$OCO$_2$Li, polyethylene carbonate (CH$_2$CH$_2$OCOO)$_n$, and polyvinylenecarbonate [poly(VC)], respectively.

Figure 12. C 1s and O 1s XPS spectra on composite graphite during initial charge (Li intercalation) process at 25°C. (a) 1 mol dm^{-3} LiPF$_6$/EC + DMC (1:1), (b) 1 mol dm^{-3} LiPF$_6$/EC + DMC (1:1) +2 wt % VC.

peak at 285.8 eV related to CH_2CH_2O in the SEI layer is higher than that at 291 eV (CO_3) and 288 eV (CH_2O). When the SEI layer is (CH$_2$OCO$_2$Li)$_2$, the C 1s ratio of the peaks at 288 and 291 eV is 1:1. Lithium ethyl carbonate (CH$_3$CH$_2$OCO$_2$Li) has a peak ratio of 1:1:1 corresponding to CH$_3$ (286 eV), CH$_2$ (288 eV), and CO$_3$ (291 eV), as shown in Fig. 11c. According to Reactions 3 and 4, the reduction of DMC would produce the SEI layer such as CH$_3$OCO$_2$Li and CH$_3$OLi. The CH$_3$ group would be detected at 286 eV. However, the SEI layer in LiPF$_6$/EC was also detected around 286 eV. Some groups reported that the peak around 286 eV is related to polymer species.[37,38] An NMR study of the dissolved SEI solution in the EC-based electrolyte supports not only lithium ethylenedicarbonate (CH$_2$OCO$_2$Li)$_2$ but also polymer species such as poly(ethylene oxide) and polyalkylcarbonate.[35] We also believe that the SEI layer in the EC-based electrolyte contains polymer constituents. Furthermore, the VC-containing electrolyte produces the SEI layer of poly (VC) by the reductive decomposition of VC.

To analyze the formation process of the SEI layer, XPS measurements of the SEI layer formed on the composite graphite anode were carried out, as shown in Fig. 12. For the EC-based electrolyte, the SEI layer formed at 0.6 V showed lithium alkyl carbonate. The surface of the graphite at the potential (0.05 V vs. Li/Li$^+$) of LiC$_{12}$ was entirely covered with the SEI layer, because a peak at 284.3 eV related to graphite could not be seen. In addition, a peak was detected related to alkyl lithium (RLi) at 283.6 eV. However, on the top layer of the SEI at 0.05 V vs. Li/Li$^+$, the peak related the RLi species could not be observed. The peak at 285.8 eV due to polymer species increased with the intercalation of lithium. On the other hand, poly (VC) was formed on the composite graphite at 1.0 V (vs. Li/Li$^+$) in the VC-added electrolyte (Fig. 12b). The result by XPS gave good agreement with the reduction behavior in the CVs. As well as the VC-free electrolyte, the peak related to RLi at 283.6 eV was detected in the SEI layer formed on graphite at a potential of 0.05 V (vs. Li/Li$^+$). Aurbach *et al.* reported that a carbon peak around 283.5 eV could be assigned to be a carbide species such as LiCH$_3$CH$_2$OCO$_2$Li by the reduction of EC.[29] The spectrum related to the VC-free electrolyte has the carbide species peak. The VC-containing electrolyte did not have the carbide species peak. The C 1s XPS spectra obtained at a potential of 0.05 V (vs. Li/Li$^+$) showed the carbide species peak at 283.8 eV, as shown in Fig. 12b. These results suggest that the VC-containing electrolyte forms carbide species as the inner layer of the SEI.

The XPS measurement with Ar$^+$ ion sputtering has been used to obtain the depth information of the SEI layer. One must watch for damage to the sample by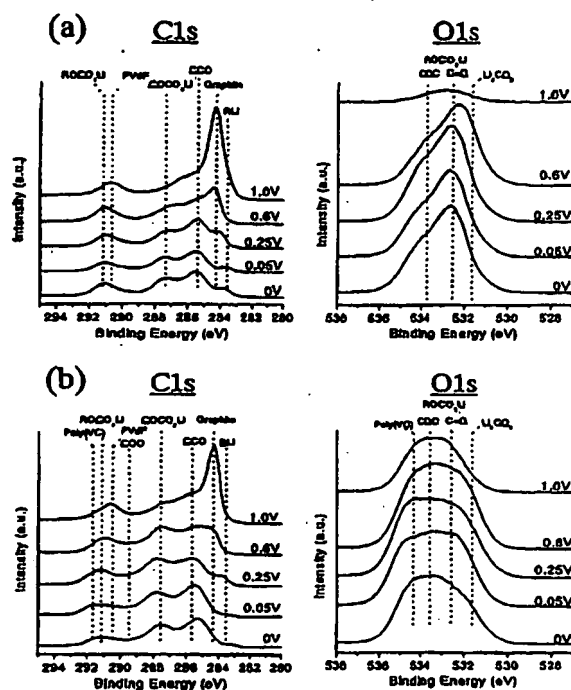 the Ar$^+$ ion sputtering, because almost all organic compounds are reduced by sputtering. Moreover, Ar$^+$ ion sputtering in the composite graphite anode may produce inhomogeneous etching because of the higher degree of roughness. The HOPG anode, which has a smooth plane, can be homogeneously sputtered. Figure 13 shows the O 1s and F 1s XPS spectra of the SEI layer formed on the HOPG basal plane with Ar$^+$ ion sputtering. The XPS spectra of the SEI layer in the VC-containing electrolyte after Ar$^+$ ion sputtering for 5 min did not show peaks attributed to poly (VC), ROCO$_2$Li, and LiF. These results indicate that the VC-derived SEI layer is a thinner film compared to the SEI layer in the VC-free electrolyte. Figure 14 shows SEM images of the SEI layers formed on the HOPG basal plane at 25°C. We observed the SEI layer formed after the first lithium intercalation-deintercalation. The SEM image of the SEI layer in the VC-containing electrolyte showed a very smooth surface morphology, as shown in Fig. 14b. The VC-free derived SEI layer (Fig. 14a) had a nonhomogeneous morphology. Matsuoka *et al.* reported that the SEI layer formed on the HOPG basal plane in LiPF$_6$/EC + EMC with 2 wt % VC was a thinner film of less than 1.0 nm based on an *ex situ* AFM study.[30] The XPS spectra in the VC-containing electrolyte showed a thickness of more than several nanometers, because a peak related to the carbon of HOPG was not detected in the C 1s spectrum before Ar$^+$ ion sputtering. The detected XPS region in this XPS measurement is from about 4 to 5 nm. It is considered that the thickness of the SEI layer is controlled by the SEI forming conditions such as electrolyte component, kind of anode, charging rate, and temperature. Although the thickness of the VC-derived SEI layer differed, it corresponded to suppressing an increase in the SEI layer by adding VC to the EC-based electrolyte in the HOPG anode.
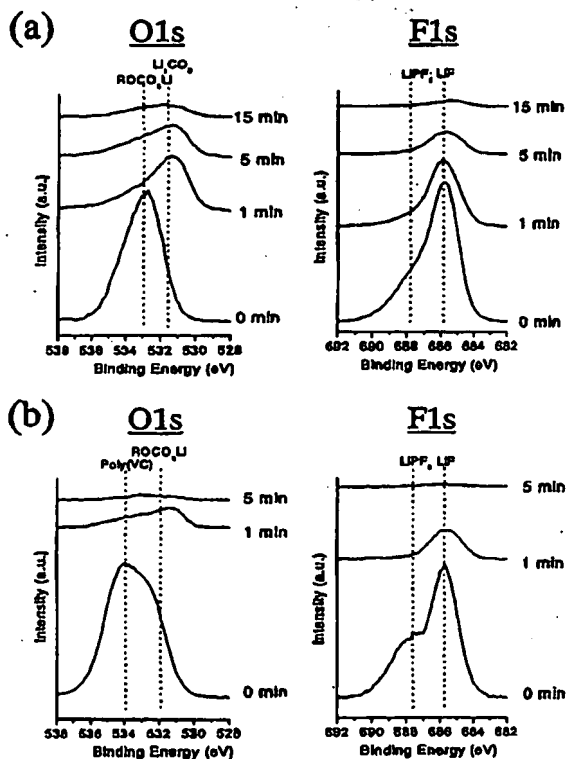
Figure 13. O 1s and F 1s XPS spectra with Ar⁺ ion sputtering of SEI layer formed on the HOPG basal plane in (a) 1 mol dm⁻³ LiPF₆/EC + DMC (1:1) and (b) 1 mol dm⁻³ LiPF₆/EC + DMC (1:1) +2 wt % VC at 25°C.

Figure 14. SEM images of SEI layers formed on the HOPG basal plane in (a) 1 mol dm⁻³ LiPF₆/EC + DMC (1:1) and (b) 1 mol dm⁻³ LiPF₆/EC +DMC (1:1)+2% VC at 25°C.

Analysis of the VC derived SEI layer by FTIR spectroscopy.—Figure 15 compares the FTIR spectra measured from the composite graphite anode after the first lithium intercalation-deintercalation in (a) LiPF₆/EC + DMC, (b) LiPF₆/EC + DMC + 2 wt % VC, and (c) LiPF₆/VC. The FTIR spectra of the SEI layers in the EC-based electrolytes showed peaks at 1647 cm⁻¹ ($\nu_{asC=O}$), 1400 cm⁻¹ ($\delta_{CH3,CH2}$), 1317 cm⁻¹ ($\nu_{sC=O}$), 1074 cm⁻¹ ($\nu_{C=O}$), and 820 cm⁻¹ (δ_{OCO2}^-). These peaks are attributed to lithium alkyl carbonate (ROCO₂Li) species as the major reduction products of the EC solvent.[29] The VC-containing electrolyte and the VC-only electrolyte have some peaks related to poly (VC) at 1817, 1147, 1080, and 758 cm⁻¹. Compared to the FTIR spectrum of VC (Fig. 15g), that of poly (VC) consists of broad peaks, as shown in Fig. 15f. Furthermore, the VC derived SEI layers contain peaks related to carboxylate (COO⁻M⁺) at 1580 cm⁻¹ (ν_{CO2}^-) and 1413 cm⁻¹ (ν_{CO2}^-). Figure 15d shows the FTIR spectrum of lithium acetate (CH₃COOLi). The carboxylate has a strong peak around 1580 cm⁻¹ and a medium peak around 1400 cm⁻¹ in the FTIR spectrum. It is considered that the counter cation of the carboxylate could be the lithium ion. In addition to poly (VC) and RCOOLi, the VC-derived SEI layers have a carbon double bond (C=C), which has peaks around 1620 cm⁻¹ ($\nu_{C=C}$) and 972 cm⁻¹ ($\delta_{C=C-O}$). We estimate that the structure of the C=C—O unit consists of VC reduction products such as lithium vinylene carbonate (C=COCO₂Li) and lithium vinylene alkoxide (C=COLi).

Analysis of the VC derived SEI layer by TOF-SIMS.—TOF-SIMS uses a pulsed high-energy ion beam to probe the surface. The primary ion beam strikes the surface of the sample, transferring energy to the surface species. Some of these secondary species are charged and have sufficient energy to escape the surface. These secondary ions are subsequently analyzed by mass spectrometry. TOF-SIMS has been recognized as a surface analysis method. TOF-SIMS can give information about the surface molecular weights of polymers in the high mass range. Because TOF-SIMS is a very sensitive technique for surface analysis, care must be taken to avoid contamination. The electrolyte on the SEI layer was removed with highly purified DME. Figure 16 shows the TOF-SIMS spectra (positive ion) for the SEI layers formed on the HOPG basal plane. The TOF-SIMS spectrum of the SEI layer in the VC-containing electrolyte exhibited mass peaks of m/z 13(CH), 26(C₂H₂) related to the C=C unit around m/z 100-250. The C=C unit could contribute to polyacetylene. We estimated that acetylene due to the reduction of VC polymerizes on the anode because acetylene has a high reactivity characteristic. However, the FTIR spectrum of the SEI layer in the VC-containing electrolyte did not exhibit peaks related to polyacetylene. It is considered that polyacetylene exists only on top of the layer. As described in the evolved gas analysis, we consider that the formation of acetylene is low because acetylene could be polymerized on the graphite anode.

SEI formation of VC.—Based on the NMR, FTIR, and XPS studies, poly (VC) was detected as the VC derived SEI layer. The oligomer component of VC was confirmed by NMR. The evolved gas species during the initial charging process were mainly CO₂. We considered that CO₂ was formed by decarbonation via the reduction of VC. Furthermore, CO₂ may produce lithium carboxylate (RCOOLi), which was confirmed by FTIR and XPS. The FTIR re-

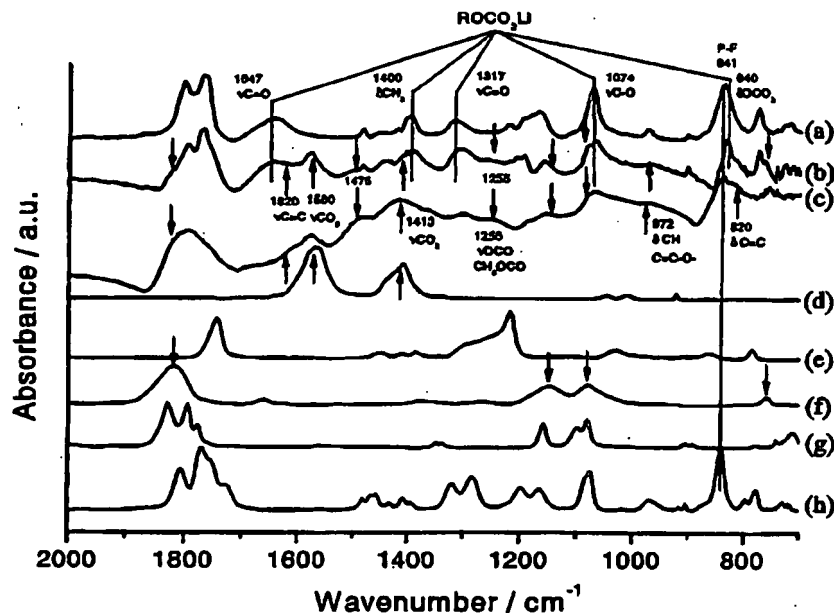Figure 15. FTIR spectra of SEI layers formed on composite graphite in (a) 1 mol dm^{-3} LiPF$_6$/EC + DMC (1:1), (b) 1 mol dm^{-3} LiPF$_6$/EC + DMC (1:1) + 2 wt % VC, and (c) 1 mol dm^{-3} LiPF$_6$/VC. Spectra (d), (e), (f), (g), and (h) are lithium acetate (CH$_3$COOLi), polyethylene carbonate (CH$_2$CH$_2$OCOO)$_n$, poly(VC), VC, and 1 mol dm^{-3} LiPF$_6$/EC + DMC (1:1) + 2 wt % VC, respectively.

sults indicated the existence of the C=C—O unit. When the combination between the double bond carbon and oxygen of carbonate is broken by reductive decomposition, lithium vinylene carbonate forms as the SEI layer. For lithium vinylene dicarbonate (CHOCO$_2$Li)$_2$, acetylene simultaneously forms as a gas component, as in the following equation

Figure 16. TOF-SIMS spectra of SEI layers formed on the HOPG basal plane in (a) 1 mol dm^{-3} LiPF$_6$/EC + DMC (1:1) and (b) 1 mol dm^{-3} LiPF$_6$/EC + DMC (1:1) + 2 wt % VC at 25°C.

$$2VC + 2e^- + 2Li^+ \rightarrow LiO_2COC\equiv COCO_2Li + C_2H_2 \quad [6]$$

On the other hand, lithium divinylene dicarbonate (CH=CHOCO$_2$Li)$_2$ cannot form acetylene, as shown in the following equation

$$2VC + 2e^- + 2Li^+ \rightarrow LiO_2COC\equiv C—C\equiv COCO_2Li \quad [7]$$

From the evolved gas results in LiPF$_6$/VC, CO gas was generated as a reductive gas of VC. CO would contribute to SEI formation of lithium divinylene dialkoxide (CH=CHOLi)$_2$, as in the following equation

$$2VC + 2e^- + 2Li^+ \rightarrow LiOC\equiv C—C\equiv COLi + 2CO \quad [8]$$

As described in the evolved gas analysis and TOF-SIMS results, we consider that the formation of acetylene is low because acetylene could be polymerized on the graphite anode. In addition to poly (VC), the VC oligomer, and polyacetylene, another polymer component was found by NMR.

Thermal stability of battery using the three-electrode cell.—The cell using the VC-containing electrolyte showed good performance at elevated temperature. We evaluated the thermal stability of batteries using three-electrode cells to analyze the behavior of the electrodes. Figure 17 shows OCV profiles of the LiCoO$_2$/graphite ion cells in the fully discharged state (SOC 0%). The OCV of the LiCoO$_2$/graphite cell was decreased over time by holding at 60°C. The OCV profile of the LiCoO$_2$/graphite cell in the VC-containing electrolyte was stable compared to that of the VC-free electrolyte. Although the OCV of LiCoO$_2$ vs. Li/Li$^+$ was very stable, the OCV of graphite vs. Li/Li$^+$ increased over time. These results suggest that the contribution of OCV changes in LiCoO$_2$/graphite cells caused by storage at 60°C in the SOC 0% state occurs mainly on the graphite anode side, not the LiCoO$_2$ cathode side. The graphite anode showed a potential of 0.7 V (vs. Li/Li$^+$) by the existence of the SEI layer on the graphite anode. The graphite anode's potential in the VC-free and VC 2% electrolytes after storage for 3 days at 60°C
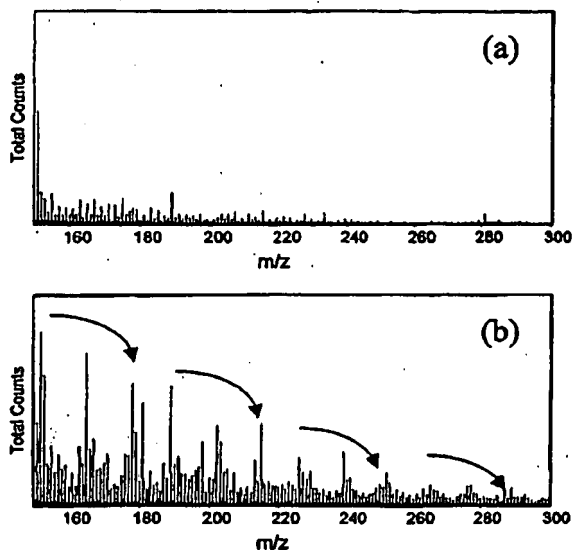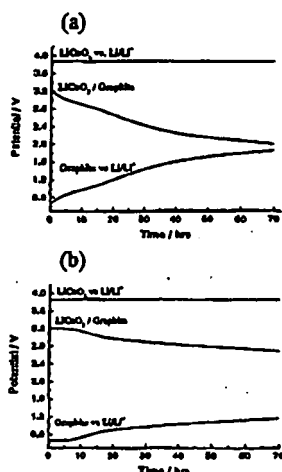
Figure 17. OCV profiles of the LiCoO$_2$/graphite ion cells at fully discharged state in (a) 1 mol dm^{-3} LiPF$_6$/EC + DMC (1:1) and (b) 1 mol dm^{-3} LiPF$_6$/EC + DMC (1:1) + 2 wt % VC. The OCV profiles of LiCoO$_2$/graphite, LiCoO$_2$ vs. Li/Li$^+$, and graphite vs. Li/Li$^+$ were recorded at 60°C.

Figure 18. TPD profiles of SEI layer on composite graphite in (a) 1 mol dm^{-3} LiPF$_6$/EC + DMC (1:1) and (b) 1 mol dm^{-3} LiPF$_6$/EC + DMC (1:1) + 2 wt % VC: (1) before and (2) after storage for 3 days at 60°C.

showed 1.2 and 1.9 V (vs. Li/Li$^+$), respectively. The increase of potential by storage at 60°C was related to decomposition of the SEI layer on the graphite. Next, we analyzed the thermal stability of the SEI layer formed on composite graphite.

Thermal stability of the VC derived SEI layer by TPD-MS.— TPD-MS was used to analyze the thermal stability of the SEI layer formed on composite graphite. The SEI layer formed on composite graphite in the LiPF$_6$/EC + DMC (1:1) electrolyte before storage at 60°C decomposed at 130°C. By adding VC to LiPF$_6$/EC + DMC (1:1), the thermal stability of the SEI layer shifted to a higher temperature. In the TPD-MS measurement, the fact that the graphite anode before charging did not show the CO$_2$ peak was related to the thermal decomposition of the electrolyte. Therefore, this clearly shows that the CO$_2$ peak is due to the decomposition gas of the SEI layer. The CO$_2$ peak of the SEI layer in the VC-free electrolyte after storage for 3 days at 60°C was greatly reduced. However, the CO$_2$ peak of the SEI layer in the VC-containing electrolyte was slightly reduced. Decomposition of the SEI layer in the VC-free electrolyte occurred around 50°C, as shown in Fig. 18-1a. During storage at 60°C, the organic carbonate SEI layer would decompose over time. Therefore, we consider that the CO$_2$ peak related to ROCO$_2$Li decreases by storage at 60°C. The TPD profile in VC-containing electrolyte after storage was stable compared to that in VC-free electrolyte owing to the high thermal stability of the VC derived SEI layer. The VC additive shows good performance on high-temperature storage. We believe that the battery performance at elevated temperatures is related to the thermal stability of the SEI layer. When the SEI layer is broken, the surface of the graphite anode could react with the electrolyte. As a result, it tends to have a decreasing battery capacity due to an unwanted reaction.

Conclusions

In this study, we investigated the SEI layers formed on the graphite in a VC-containing electrolyte using evolved gas analysis, TOF-SIMS, FTIR spectroscopy, XPS, TPD-MS, SEM, and NMR. The presence of VC in the EC-based electrolyte caused decreased reductive gases of the EC-DMC solvent such as C$_2$H$_4$, CH$_4$, and CO. The VC-derived SEI layer formed at a potential more positive
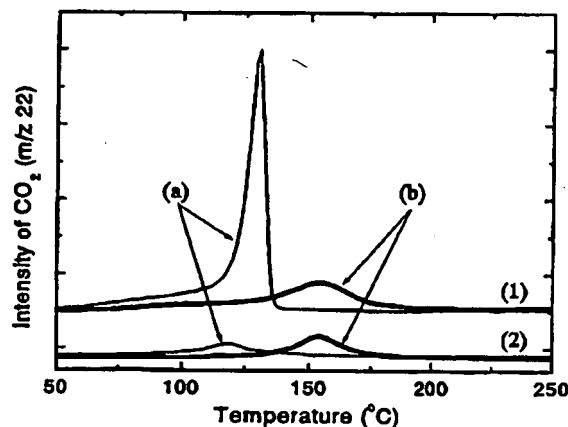
than 1.0 V vs. Li/Li$^+$. The reductive gas of VC was mainly CO$_2$. Effective SEI formation by reduction of VC at the graphite anode occurs before that of EC. The VC derived SEI layers consist of polymer species such as poly (VC), the oligomer of VC, the ring-opening polymer of VC, and polyacetylene. CO$_2$ formation in the battery using the electrolyte containing VC has no relation to the poly (VC) and VC oligomer formation because these polymer structures maintain carbonate units. We consider that CO$_2$ formation is due to the decarboxylation of VC. Moreover, lithium vinylene dicarbonate (CHOCO$_2$Li)$_2$, lithium divinylene dicarbonate (CH=CHOCO$_2$Li)$_2$, lithium divinylene dialkoxide (CH=CHOLi)$_2$, and lithium carboxylate (RCOOLi) were formed on the graphite as VC reduction products. The thermal stability of batteries using the three-electrode cells was evaluated to analyze the behavior of the electrodes. From the results using the three-electrode cell, the battery performance at elevated temperature would be mainly controlled by the graphite anode side. We demonstrate that the VC derived SEI layer has excellent thermal stability using TPD-MS. In VC-free electrolyte, the SEI layer is partially destroyed during high-temperature storage. However, the VC-derived SEI layer is maintained at a high temperature because of good thermal stability. When the SEI layer that has formed on the graphite anode is broken, SEI formation occurs to repair the SEI layer. This leads to decreased battery capacity due to an unwanted reaction. The excellent thermal stability due to the VC derived SEI layer on the graphite anode has a close relation to the battery performance at elevated temperatures.

References

1. L. J. Krause, W. Lamanna, J. Summerfield, M. Engle, G. Korba, R. Loch, and R. Atanasoski, *J. Power Sources*, **68**, 320 (1997).
2. W. Xu and C. A. Angell, *Electrochem. Solid-State Lett.*, **4**, E1 (2001).
3. M. Schmidt, U. Heider, A. Kuehner, R. Oesten, M. Jungnitz, N. Ignat'ev, and P. Sartori, *J. Power Sources*, **97-98**, 557 (2001).
4. P. Kita, H. Sakata, A. Kawakami, H. Kamizori, T. Sonoda, H. Nagashima, N. V. Pavlenko, and Y. L. Yagupolskii, *J. Power Sources*, **97-98**, 581 (2001).
5. Y. Sasaki, M. Handa, K. Kurashima, T. Tonuma, and K. Usami, *J. Electrochem. Soc.*, **148**, A999 (2001).
6. O. Chusid, Y. Ein Ely, D. Aurbach, M. Babai, and Y. Carmeli, *J. Power Sources*, **43**, 47 (1993).
7. J. O. Besenhard, M. W. Wagner, M. Winter, A. D. Jannakoudakis, P. D. Jannakoudakis, and E. Theodoridou, *J. Power Sources*, **44**, 413 (1993).
8. D. Aurbach, Y. Ein-Eli, O. Chusid, Y. Carmeli, M. Babai, and H. Yamin, *J. Electrochem. Soc.*, **141**, 603 (1994).

9. J. O. Besenhard, M. Winter, J. Yang, and W. Biberacher, *J. Power Sources*, 54, 228 (1995).
10. S. Komaba, B. Kaplan, T. Ohtsuka, Y. Kotaoka, N. Kumagai, and H. Groult, *J. Power Sources*, 119-121, 378 (2003).
11. C. Jehoulet, P. Biensan, J. M. Bodet, M. Broussely, C. Moteau, and C. Tessier-Lescourret, in *Batteries for Portable Applications and Electric Vehicles*, A. R. Landgrebe and C. P. Holmes, Editors, PV 97-18, p. 974, The Electrochemical Society Proceedings Series, Pennington, NJ (1997).
12. C. Wang, H. Nakamura, H. Komatsu, M. Yoshio, and H. Yoshitake, *J. Power Sources*, 74, 142 (1998).
13. H. Yoshitake, K. Abe, T. Kitakura, J. B. Gong, Y. S. Lee, H. Nakamura, and M. Yoshio, *Chem. Lett.*, 32, 134 (2003).
14. K.-C. Möller, H. J. Santner, W. Kern, S. Yamaguchi, J. O. Besenhard, and M. Winter, *J. Power Sources*, 119-121, 561 (2003).
15. H. J. Santner, K.-C. Möller, J. Ivanco, M. G. Ramsey, P. P. Netzer, S. Yamaguchi, J. O. Besenhard, and M. Winter, *J. Power Sources*, 119-121, 368 (2003).
16. G. H. Wrodnigg, J. O. Besenhard, and M. Winter, *J. Electrochem. Soc.*, 146, 470 (1999).
17. G. H. Wrodnigg, T. M. Wrodnigg, J. O. Besenhard, and M. Winter, *Electrochem. Commun.*, 1, 148 (1999).
18. Y. Ein-Eli, S. R. Thomas, and V. R. Koch, *J. Electrochem. Soc.*, 144, 1159 (1997).
19. Y. Ein-Eli, *J. Electroanal. Chem.*, 531, 95 (2002).
20. Z. X. Shu, R. S. McMillan, J. J. Murray, and I. J. Davidson, *J. Electrochem. Soc.*, 143, 2230 (1996).
21. R. McMillan, H. Slegr, Z. X. Shu, and W. Wang, *J. Power Sources*, 81-82, 20 (1999).
22. Z. X. Shu, R. S. McMillan, and J. J. Murray, *J. Electrochem. Soc.*, 140, 922 (1993).
23. M. Inaba, Y. Kawatate, A. Funabiki, S.-K. Jeong, T. Abe, and Z. Ogumi, *Electrochim. Acta*, 45, 99 (1999).
24. A. Naji, J. Ghanbaja, P. Willmann, and D. Billaud, *Electrochim. Acta*, 45, 1893 (2000).
25. K.-C. Möller, T. Hodal, W. K. Appel, M. Winter, and J. O. Besenhard, *J. Power Sources*, 97-98, 595 (2001).
26. Y. Matsuo, K. Fumita, T. Fukutsuka, Y. Sugie, H. Koyama, and K. Inoue, *J. Power Sources*, 119-121, 373 (2003).
27. H. Ota, A. Kominato, W.-J. Chun, E. Yasukawa, and S. Kasuya, *J. Power Sources*, 119-121, 393 (2003).
28. P. Biensan, J. M. Bodet, F. Perton, M. Broussely, C. Jehoulet, S. Barusseau, S. Herreyre, and B. Simon, Paper 286 presented at The 10th International Meeting on Lithium Batteries, Como, Italy, May 28-June 2, 2000.
29. D. Aurbach, K. Gamolsky, B. Markovsky, Y. Gofer, M. Schmidt, and U. Heider, *Electrochim. Acta*, 47, 1423 (2002).
30. O. Matsuoka, A. Hiwara, T. Omi, M. Toriida, T. Hayashi, C. Tanaka, Y. Saito, T. Ishida, H. Tan, S. S. Ono, and S. Yamamoto, *J. Power Sources*, 108, 128 (2002).
31. X. Zhang, R. Kostecki, T. J. Richardson, J. K. Pugh, and P. N. Ross, Jr., *J. Electrochem. Soc.*, 148, A1341 (2001).
32. S.-K. Jeong, M. Inaba, R. Mogi, Y. Iriyama, T. Abe, and Z. Ogumi, *Langmuir*, 17, 8281 (2001).
33. Y. Wang, S. Nakamura, K. Tasaki, and P. B. Balbuena, *J. Am. Chem. Soc.*, 124, 4408 (2002).
34. Y. Wang and P. B. Balbuena, *J. Phys. Chem. B*, 106, 4486 (2002).
35. H. Ota, Y. Sakata, X. Wang, J. Sasahara, and E. Yasukawa, *J. Electrochem. Soc.*, 151, A437 (2004).
36. E. Peled, D. Bar Tow, A. Merson, A. Gladkich, L. Burstein, and D. Golodnitsky, *J. Power Sources*, 97-98, 52 (2001).
37. D. Bar-Tow, E. Peled, and L. Burstein, *J. Electrochem. Soc.*, 146, 824 (1999).
38. A. M. Andersson and K. Edström, *J. Electrochem. Soc.*, 148, A1100 (2001).

Experimental and theoretical studies on reduction mechanism of vinyl ethylene carbonate on graphite anode for lithium ion batteries

Yongsheng Hu, Weihe Kong, Hong Li, Xuejie Huang, Liquan Chen *

Laboratory for Solid State Ionics, Institute of Physics, Chinese Academy of Sciences, P.O. Box 603, Beijing 100080, China

Abstract

Vinyl ethylene carbonate (VEC) has been investigated as an electrolyte additive for use in lithium ion batteries. Even in small additive amounts (5 vol%) VEC was capable of preventing propylene carbonate (PC) co-intercalation into graphite. The formation of a stable passivating film on the graphite surface is believed to be the reason for the improved cell performance. The passivating film resulting from the reductive decomposition of VEC on the graphite surface was comprehensively studied by FTIR and XPS as well as the density functional theory (DFT) calculations.
© 2003 Elsevier B.V. All rights reserved.

Keywords: Vinyl ethylene carbonate; Electrolyte additive; Density functional theory; Lithium ion batteries

1. Introduction

Due to the growing demands for portable electronic devices and electric vehicles (EV), lithium ion batteries are undergoing rapid development aimed at higher energy density and cycling stability [1,2]. With a series of excellent properties such as low melting point (224.2 K), high dielectric constant, high chemical stability toward metallic lithium and wide electrochemical window, propylene carbonate (PC) is still an attractive candidate of solvent for non-aqueous electrolytes for lithium ion batteries at both high and low temperatures. Unfortunately, PC molecules and solvated Li^+ ions can co-intercalate into graphite, accompanied with severe exfoliation of graphite layers and destruction of the graphite structure. Many methods have been developed to suppress the solvent co-intercalation into graphite. One of these is to employ film-forming additives that predominantly react on the graphite surfaces in the first cycling process [3,4]. Vinylene

carbonate (VC) was widely regarded as a highly reactive additive for forming passivating films on the surface of graphite anodes in lithium ion batteries [1,5,6]. However, VC is known as an unstable compound because it tends to polymerization [1,5–7]. In this paper, we introduced the vinyl ethylene carbonate (VEC) as electrolyte additive for non-aqueous electrolyte-based lithium ion batteries. Comparing its structural formula with VC (in Fig. 1), VEC is supposed to be more stable than VC because the double bond of VEC is somewhat electron rich, thus not very reactive towards double bonds, whereas the ester group directly bonding with the vinyl group in VC is electron withdrawing enough to make it a little less electron rich, leading to highly reactive towards double bonds [8]. FTIR and XPS were widely used to determine compositions of the surface film on the Li or graphite electrodes. Nevertheless, they alone cannot provide specific enough information which enables a completed chemical analysis of surface species. Here, a comprehensive study of the film resulting from the reductive decomposition of VEC by FTIR and XPS combined with DFT calculations may be much more conclusive than using each method alone.

* Corresponding author. Tel./fax: +86-10-82649046.
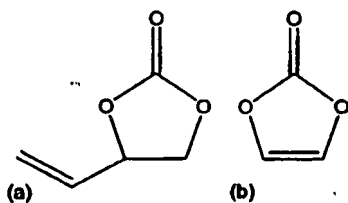E-mail address: lqchen@aphy.iphy.ac.cn (L. Chen).

Fig. 1. Structural formulae of (a) vinyl ethylene carbonate and (b) vinylene carbonate.

2. Experimental and computational details

PC (Beijing Phylion Battery Company, battery grade) was low-pressure distilled prior to use. It should be noted that the VEC (Aldrich, 99%) was highly pure and did not contain any necessary stabilizer. Lithium bis(perfluoroethysulfonyl)imide (LiBETI) (3M Company, battery grade) was dried under vacuum at 140 °C for several days. The carbon electrode was prepared from synthetic graphite powder (Timical, SLP30) by slurrying the carbon material with a solution of PVDF (10 wt%) dissolved in N-methyl-2-pyrrolidinone (NMP). The mixture was spread onto copper foil (12 μm thick) and dried at 100 °C under vacuum for 24 h.

The constant current charge-discharge experiments were carried out with current density of 0.156 mA cm^{-2} for the graphite electrode using a two-electrode cell and lithium foil as a counter electrode on a Land Celltest. The cyclic voltammogram (CV) measurements were carried out using a three-electrode cell on a CHI660a electrochemical workstation with graphite electrode as the working electrode and lithium foils (99.9%) as both the counter and reference electrodes. All of the cells were assembled and disassembled in an argon-filled Mbraun Labmaster 130 glove box (H$_2$O <1 ppm). The graphite electrodes after cycling were rinsed with anhydrous DMC (Beijing Phylion Battery Company, battery grade) to remove the electrolyte residue and then were evacuated in the chamber of the glove box for 24 h to remove DMC. The graphite powder scratched from the graphite electrode was mixed with dry KBr and pressed into pellet for FTIR measurement, carried out on a Bio-RAD FTS-60V spectrometer using a transmittance mode. The resolution of the spectrometer was set at 2 cm^{-1}. XPS measurement was performed on a VG MKII XPS spectrometer, base pressure = 10^{-9} Torr, using a monochromatized Al Kα source. The Au powder was pressed on the graphite electrode after rinse and used as energy calibration. A depth profile was obtained by Ar$^+$ ion beam sputtering (2 keV).

All the calculations have been performed using the Gaussian 98 program package [9]. The equilibrium and transition structures were fully optimized by B3PW91 method using 6-311++G(d,p) basis set [10]. Single-point

energies for the B3PW91/6-311++G(d,p) optimized geometries have also been calculated at the same level. To confirm the transition states and make zero point energy (ZPE) corrections, frequency analyses and primary intrinsic reaction coordinate (IRC) calculations were done with the same basis set as for the geometry optimization.

3. Results and discussion

3.1. Electrochemical characterizations

Fig. 2 shows the voltage-time profiles of graphite/Li cells without and with electrolyte additive in the first two cycles. For the cell without an additive, only a long discharge plateau at ca. 0.9 V (Fig. 2(a)) was observed, due to the co-intercalation of PC and the solvated Li$^+$ ions into graphite. The electrode potential cannot reach the potential for intercalation of unsolvated Li$^+$ ions (<0.25 V vs. Li/Li$^+$). In contrast, in case of addition of 5 vol% VEC, there is no long discharge plateau at ca. 0.9 V in the discharge curve. Addition of VEC into the electrolyte completely changes the voltage profile of graphite/Li cell. It drops rapidly at the beginning, then followed by a slow decrease between 1.3 and 0.2 V. Below 0.2 V, the Li$^+$ ions are intercalated into graphite. Electrolyte decomposition takes place on the graphite electrode between 1.3 and 0.2 V. This results in the formation of a passivating film on the graphite surface. This film is usually regarded as the solid electrolyte interface (SEI) [11–13]. It is ionically conductive and electronically insulating. Moreover, the CV profiles clearly show the effect of VEC additive, which suppresses greatly the co-intercalation and exfoliation of graphite. In case of no additive into the electrolyte, the co-intercalation of PC and solvated Li$^+$ ions began at ca. 0.9 V in Fig. 3(a) and the cathodic current became much larger in the lower potential direction, and eventually, no anodic peak due to delithium was observed during reverse scanning. However, when added 5 vol%
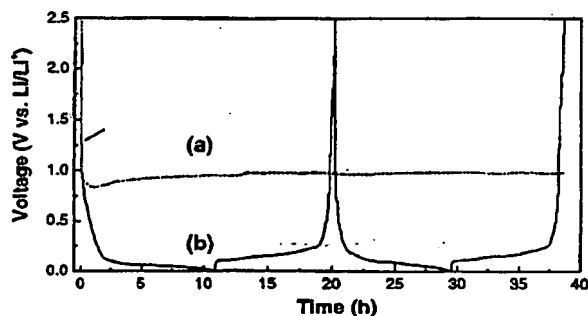

Fig. 2. Voltage-time profiles of the first two cycles of graphite/Li cells using (a) 1 M LiBETI/PC and (b) 1 M LiBETI/PC/VEC (95:5 v/v) as electrolytes (C/10, i = 0.15 mA cm^{-2}, $V_{cut-off}$ is 2.5–0.01 V vs. Li/Li$^+$).
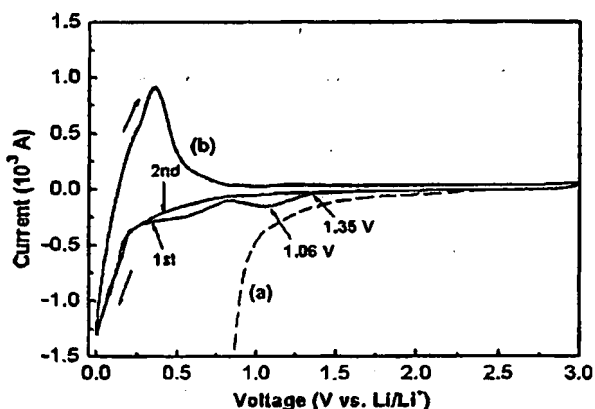
Fig. 3. Cycle voltammograms of fresh graphite electrodes in (a) 1 M LiBETI/PC and (b) 1 M LiBETI/PC/VEC (95:5 by volume) electrolytes with a scan rate of 0.1 mV/s.

Fig. 5. FTIR spectrum measured ex situ from the graphite electrode after discharging to 0.01 V in 1 M LiBETI/PC/VEC (95:5 v/v) electrolyte.
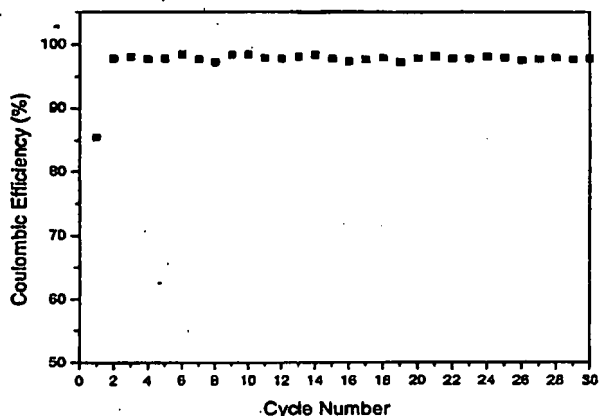

Fig. 4. Variation of the Coulombic efficiencies with cycle number for the graphite electrode in 1 M LiBETI/PC/VEC (95:5 v/v) electrolyte.

VEC, it can be observed that the very small reductive current starts to appear at 1.35 V together with a small reductive peak located at ca. 1.06 V as shown in Fig. 3(b). We attribute this reductive peak to the decomposition of VEC. Fig. 4 shows the variation of the Coulombic efficiencies with cycle number in the presence of the additive. The addition of VEC gave a good cycleability. The Coulombic efficiencies of the first, second and 30th cycles are 85%, 98% and 97.8%, respectively, suggesting that the film on the graphite surface is stable and compact. The improvement of the electrochemical performance of graphite electrode was benefited from high quality decomposition products of VEC.

3.2. Spectroscopic characterizations

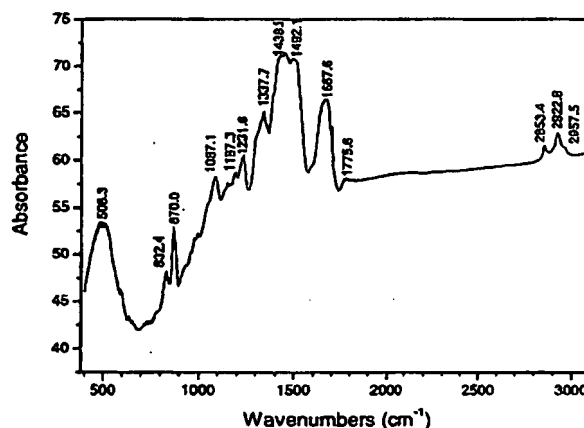Fig. 5 shows the FTIR spectrum measured ex situ from the graphite electrode after discharging to 0.01 V.

The pronounced bands around 2853.4–2957.5 cm^{-1} (vCH), 1667.4 cm^{-1}(v_{as} C=O), 1337.7 cm^{-1} (v_s C=O) and 832 cm^{-1} (δOCO$_2$) are typical of lithium alkylcarbonates (ROCO$_2$Li), which are major reduction products of alkyl carbonate solutions on Li, Li–C and noble metal electrodes polarized to low potentials in the presence of Li$^+$ ions [12–14]. It has been reported that the v_{as} C=O band shifts to higher frequency with lengthening the alkyl (R) chain in ROCO$_2$Li [14]. When R are propyl and butyl, it locates at 1650 and 1660 cm^{-1}, respectively [14]. In our case, the band locates at 1667.4 cm^{-1}, it must originate from the decomposition products of VEC. The bands present around 1435.1 to 1492.1 cm^{-1} (vCO$_3^{2-}$) and 870 cm^{-1} (δCO$_3^{2-}$) are characteristic for Li$_2$CO$_3$ while the bands at 1187.3 cm^{-1}(vC–O), 1087.1 cm^{-1}(vC–O) and 508.3 cm^{-1} (Li–O) are attributed to ROLi [12–14]. The band at 1775.6 cm^{-1} may relate either to residual solvent or to
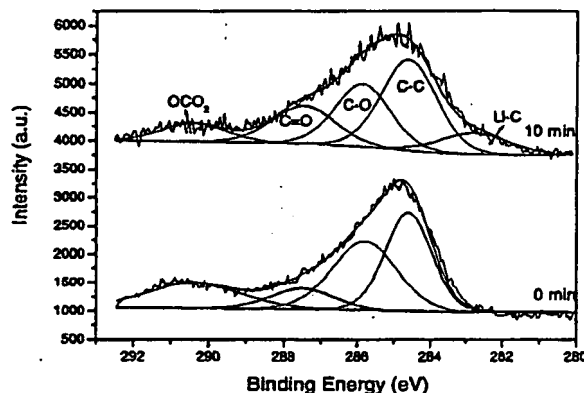

Fig. 6. Typical C1s XPS band and its deconvolution to peaks related to the various oxidation states of the C.

polycarbonate that might be formed by some polymerization of VEC. Typical XPS spectra of C1s from the graphite electrode cycled in VEC-containing electrolyte and after sputtering 10 min are shown in Fig. 6. It can be seen that it contains multicomponents due to the coexistence of different chemical states of C. XPSPEAK software is used to fit this band based on a Shirley background subtraction. The binding energies of the four fitted Gaussian-shaped components are located at 284.6, 285.8, 287.5 and 290.4 eV, corresponding to the

C–C, C–O, C=O and OCO₂ groups, respectively [15,16]. These groups are in line with the expected formation of ROCO₂Li, ROLi and Li₂CO₃ species on the graphite electrode surface. Hence, the XPS data correlate with the information obtained by the FTIR spectroscopic studies. Upon sputtering, a new peak around 282.8 eV appears. This peak, which reflects carbon at a very low oxidation state, can be attributed only to species containing C–Li bonds (RLi) [16,17]. It should be noted that FTIR spectroscopic studies of graphite electrode
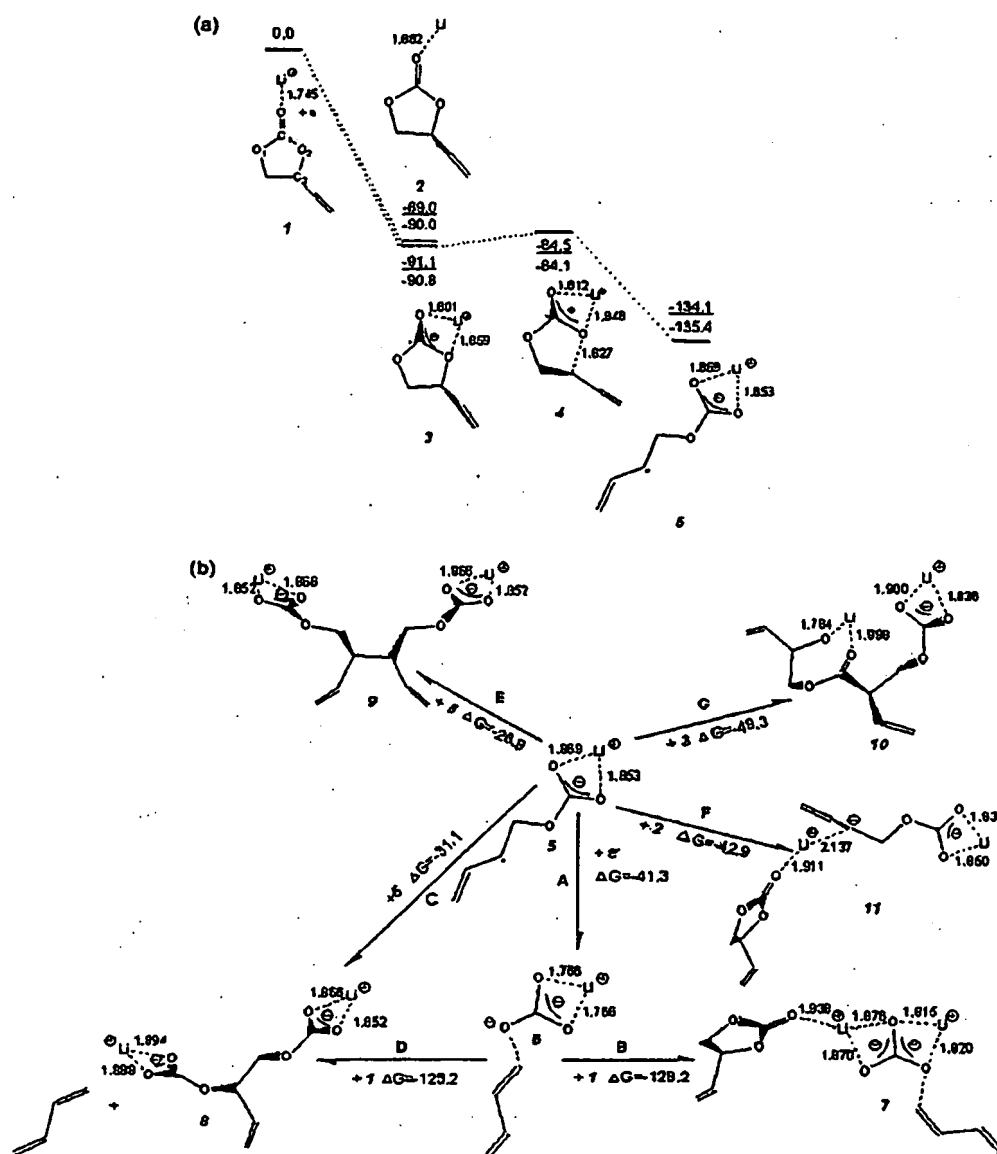

Fig. 7. (a) Potential energy (underlined data) and Gibbs free energy profile (in kcal/mol) at 298.15 K for the reductive dissociation process of Li⁺(VEC) calculated with B3PW91/6-311++G(d,p) methods. (b) Termination reactions of carbonate radical anion coordinated with Li⁺ ion for the model Li⁺(VEC).

are not capable of detecting Li carbide species. Therefore, information on the formation of surface RLi species on graphite is a unique contribution of XPS measurements.

3.3. DFT calculations on the reductive reactions of VEC

The potential energy surface and Gibbs free energy surface profiles are shown in Fig. 7(a) together with some selected structural data. The reductive decomposition of VEC initially encounters the ion-pair intermediates 2 and 3. An electron was transferred to Li^+ ion in 1 to form the intermediate 2, and to VEC in 1 to form the intermediate 3, respectively. Then, homolytic C_2–O_2 bond cleavage could happen to intermediate 3, leading to form a radical anion coordinated with Li^+ ion. The opening in 3 through a transition state 4 faces a barrier of 6.6 kcal/mol. The transition state characteristic of 4 connecting 3 with 5 was confirmed by primary IRC calculations and the sole imaginary frequency which is −841 cm^{-1}. Formation of the radical anion 5 results in much more energy releasing, −134.1 kcal/mol relative to 1. The possible termination ways of radical anion 5 are shown in Fig. 7(b). The first termination way is the further reduction by another electron transfer from the polarized electrode (Path A), by which a weak complex 6 of butadiene gas and unpaired nucleophilic carbonate anion ($LiCO_3^-$) are generated. In the GC-MS measurements, we indeed detected the butadiene gas [18]. Once the carbonate anion ($LiCO_3^-$) of 6 is formed, it may either being paired by Li^+ ion from 1 (Path B), it may precipitate as insoluble inorganic lithium carbonate, Li_2CO_3, 7, or nucleophilicly attack another Li^+(VEC), 1, to form 8, $LiO_2COCH_2CH(CH= CH_2)OCO_2Li$ (Path D). The two paths are thermodynamically very competitive as shown by their almost identical Gibbs free energies of reactions (ΔG, −125.2 vs −128.2 kcal/mol). It is expected that the probably barrier-free self-dimerizing (Paths C and E) via nucleophilicly attacking the radical center by oxygen to bring about 8, $LiO_2COCH_2CH(CH=CH_2)OCO_2Li$ (Path C), or either the radical center to form 9, $(LiO_2COCH_2CH(CH= CH_2))_2$ (Path E). Additionally, of particular interest is the possibility of forming a species containing Li-C bonds solvated by a VEC molecule, 11, $LiCH(CH=CH_2)-CH_2OCO_2Li$, via electron-pairing between 5 and a reduction intermediate 2 (Path F). The path is in line with the XPS observation. Besides these paths, the most probable reaction among the involved reactions is the path that is the combination of 5 with the reduction intermediate 3 also via electron-pairing (Path G) generates a lithium organic salt with an ester group, 10, $Li-OCH(CH=CH_2)CH_2OCOCH(CH=CH_2)CH_2OCO_2Li$, due to the lowest Gibbs free energy of the reaction ($\Delta G = -49.3$ kcal/mol). The DFT calculations are in good agreement with the FTIR and XPS results.

4. Conclusion

A new electrolyte containing VEC and PC has been investigated for a graphite electrode in lithium ion batteries. VEC shows promising performance for use as an effective film-forming electrolyte additive in lithium ion batteries. FTIR and XPS results show that the passivating film resulting from VEC reduction on the graphite surface is probably composed of $LiORCO_2ROCO_2Li$, Li_2CO_3, $LiROCO_2Li$, $(ROCO_2Li)_2$, etc. (R = alkyl group), which is further supported by the DFT calculations. The reductive decomposition of VEC initially encounters an ion-pair intermediate and then cleavages homolytically via a 6.6 kcal/mol barrier to generate a radical anion. It will undergo secondary reactions by further reduction (Path A, $LiCO_3^-$), ion-pairing (Path B, Li_2CO_3), probably barrier-free self-dimerizing (Paths C and E, $LiO_2COCH_2CH(CH=CH_2)OCO_2Li$ and $(LiO_2COCH_2-CH(CH=CH_2))_2$), and electron-pairing (Paths F and G, $LiCH(CH=CH_2)CH_2OCO_2Li$ and $LiOCH(CH=CH_2)-CH_2OCOCH(CH=CH_2)CH_2OCO_2Li$) processes.

References

[1] R. Oesten, U. Heider, M. Schmidt, Solid State Ionics. 148 (2002) 391.
[2] J. Arai, H. Katayama, H. Akahoshi, J. Electrochem. Soc. 149 (2002) A217.
[3] J.O. Besenhard, P. Castella, M.W. Wagner, Mater. Sci. Forum 91–93 (1992) 647.
[4] J.O. Besenhard, M.W. Wagner, M. Winter, A.D. Jannakoudakis, P.D. Jannakoudakis, E. Theodoridou, J. Power Sources 43–44 (1993) 413.
[5] C. Jehoulet, P. Biensan, J.M. Bodet, M. Broussely, C. Moteau, C. Tessier-Lescourret, Proc. Electrochem. Soc. 97-18 (Batteries for Portable Application and Electric Vehicles), The Electrochem. Soc. Inc., Pennington, NJ, 1997, p. 974.
[6] D. Aurbach, K. Gamolsky, B. Markovsky, Y. Gofer, M. Schmidt, U. Heider, Electrichim. Acta 47 (2002) 1423.
[7] M.S. Newman, R.W. Addlor, J. Am. Chem. Soc. 77 (1955) 3789.
[8] D.C. Webster, A.L. Crain, Prog. Organic Coatings 40 (2000) 275.
[9] M.J. Frisch, G.W. Trucks, H.B. Schlegel, G.E. Scuseria, M.A. Robb, J.R. Cheeseman, V.G. Zakrzewski, J.A. Montgomery Jr., R.E. Stratmann, J.C. Burant, S. Dapprich, J.M. Millam, A.D. Daniels, K.N. Kudin, M.C. Strain, O. Farkas, J. Tomasi, V. Barone, M. Cossi, R. Cammi, B. Mennucci, C. Pomelli, C. Adamo, S. Clifford, J. Ochterski, G.A. Petersson, P.Y. Ayala, Q. Cui, K. Morokuma, D.K. Malick, A.D. Rabuck, K. Raghavachari, J.B. Foresman, J. Cioslowski, J.V. Ortiz, A.G. Baboul, B.B.

Stefanov, G. Liu, A. Liashenko, P. Piskorz, I. Komaromi, R. Gomperts, R.L. Martin, D.J. Fox, T. Keith, M.A. Al-Laham, C.Y. Peng, A. Nanayakkara, C. Gonzalez, M. Challacombe, P.M.W. Gill, B. Johnson, W. Chen, M.W. Wong, J.L. Andres, C. Gonzalez, M. Head-Gordon, E.S. Replogle, J.A. Pople, Gaussian 98, revision A.9, Gaussian, Inc, Pittsburgh, PA, 1998.

[10] A.D. Becke, J. Chem. Phys. 98 (1993) 5648.

[11] Y. Ein-Eli, S.R. Thomas, V.R. Koch, J. Electrochem. Soc. 144 (1997) 1159.

[12] D. Aurbach, Y. Ein-Eli, A. Zaban, J. Electrochem. Soc. 141 (1994) L1.

[13] D. Aurbach, B. Markovsky, A. Shechter, Y. Ein-Eli, J. Electrochem. Soc. 143 (1996) 3809.

[14] D. Aurbach, M.L. Daroux, P.W. Faguy, E. Yeager, J. Electrochem. Soc. 134 (1987) 1611.

[15] R. Yazami, Electrochim. Acta 45 (1999) 87.

[16] D. Bar-Tow, E. Peled, L. Burstein, J. Electrochem. Soc. 146 (1999) 824.

[17] A. Schechter, D. Aurbach, H. Cohen, Langmuir 15 (1999) 3334.

[18] Y.S. Hu, W.H. Kong, H. Li, X.J. Huang, L.Q. Chen (submitted).

Purification and carbon-film-coating of natural graphite as anode materials for Li-ion batteries

Haipeng Zhao [a,b], Jianguo Ren [a], Xiangming He [a,*], Jianjun Li [a],
Changyin Jiang [a], Chunrong Wan [a]

[a] Institute of Nuclear & New Energy Technology, Tsinghua University, Beijing 100084, PR China
[b] Pingdingshan Institute of Technology, Henan 467000, PR China

Abstract

A process of modification of natural graphite materials as anode for lithium ion batteries was attempted. The process started with the treatment of natural graphite with concentrated hydrochloric acid and concentrated sulfuric acid in a thermal autoclave, followed by the in situ polymerization of resorcinol–formaldehyde resin to coat the graphite, then heat-treatment. SEM, XRD, Raman and electrochemical charge–discharge analysis showed that the surface defects and impurities on natural graphite were eliminated by purification of the concentrated acids, and carbon-film encapsulation modified the surface structure of the graphite and reduced its BET surface area. The as-obtained natural graphite sample presented an initial charge–discharge coulombic efficiency of 88.4% and a reversible capacity of 355.8 mAh g^{-1}. The proposed process paves a way to prepare a promising anode material with excellent performance with low cost of natural graphite for rechargeable lithium ion batteries.
© 2007 Elsevier Ltd. All rights reserved.

Keywords: Natural graphite; Lithium ion battery; Coating; Oxidization; Resorcinol–formaldehyde; Concentrated acid

1. Introduction

Lithium-ion batteries are widely used in consumer electronic devices such as cellular telephones, camcorders and portable computers today. There is also a strong interest in utilizing Li-ion batteries for transportation applications. The development of anode materials is of great importance in the history of lithium ion batteries. So far, a lot of anode materials have been investigated, including synthetic graphite, natural graphite, amorphous carbon, nitrides, tin oxides, tin-based alloys and some composites. However, synthetic graphite is still the dominant one available on the market. The main reason is that the electrochemical properties of other kinds of anode materials are not viable for practical applications. Furthermore, synthetic graphite, commonly employed in the anode of commercial lithium rechargeable batteries, is expensive compared to natural graphite (NG) [1], and thus much attention is directed to natural graphite. NG is endowed with graphitic structure during the evolution of nature, and does not require heat-treatment at high temperature (2800 °C) to be graphitic. However, large irreversible capacity loss and poor cycling life have been persistent problems with the wide application of natural graphite anodes [2–5]. The problems are mainly caused by the high anisotropy of the graphite surface [6], imperfect structures such as sp^3-hybridized carbon atoms, carbon chains and edge carbon atoms [7] and some impurities [8]. These structural characteristics result in profound difference in chemical and electrochemical reactivity, interaction with the solid electrolyte interphase (SEI), kinetics for lithium intercalation and de-intercalation of the basal plane and the edge plane of the graphite [9]. They can lead to the decomposition of electrolyte molecules to produce large irreversible capacity and cycling performance deterioration.

Recently, a lot of research findings [5,10–17] have confirmed that the modification of graphite is an effective approach to improve its electrochemical performance. In the case of practical application, however, there still exist some shortcomings in these findings. Profound differences, Guo et al. [10] improved cycling performance of natural graphite by coating poly(acrylonitrile) on the surface of natural graphite particles via radiation-initiated polymerization, but suffered from big initial irreversible capacity

* Corresponding author. Tel.: +86 10 89796073; fax: +86 10 89796031.
  E-mail address: hexm@tsinghua.edu.cn (X. He).

due to the thick amorphous carbon layer with a lot of micropores and/or nanochannels. Yu and Wu coated the surface of graphite with pyrolytic carbons from pyrolysis of phenol–formaldehyde resin [13], but it was unavoidable that some resin was not coated on the graphite and formed unwanted amorphous carbon. The oxidation of graphite could modify its electrochemical performance as anode material for lithium ion batteries, but the degree of improvement was different depending on the used graphite [3]. For natural graphite, the results obtained only by oxidation cannot meet practical application demand.

Even though, the natural graphite should possibly become a practical anode material for Li-ion cells due to its low cost. In this study, a process to improve the electrochemical performance of natural graphite was proposed. Natural graphite was treated with concentrated hydrochloric acid and concentrated sulfuric acid in a thermal autoclave, followed by a coating with resorcinol–formaldehyde resin polymerized in situ on the purified graphite surface, followed by a heat-treatment. As-obtained material showed an admirable cycling performance and a high initial coulombic efficiency.

2. Experimental

The spherical natural graphite powder (Luoyang guanqi Ltd., Henan province, PR China) and a blended aqueous solution containing 36% hydrochloric acid and 98% sulfuric acid in a weight ratio of 1:10 were mixed in an autoclave, and then the autoclave was put in a muffle oven. Purification of natural graphite in the autoclave was performed at about 200 °C for 10 h. After purification, the mixture in autoclave was separated by centrifuge, rinsed and dried, successively.

The as-purified graphite powder and de-ionized water in a weight ratio of 1:20 were mixed in a four-necked flask under the condition of vigorous stirring. Then a mixture of reagent-grade resorcinol, formaldehyde, inorganic catalyzer and surfactant (Emulsifier Span-80, Sorbitan monooleate, $C_{24}H_{44}O_6$) was added into the flask. The temperature of the reaction system was controlled at 25 °C for 10 h to maintain an interfacial polymerization between water and the organic phase preferably on the surface of graphite particles. After the reactions, the mixture in the flask was separated by centrifuge to obtain a polymer-coated graphite powder, which was then washed with copious amounts of de-ionized water and vacuum dried at 60 °C for 24 h. Then the powder was heat-treated at 800 °C for 1 h in nitrogen atmosphere to make the polymer resin coated on graphite pyrolyzed into an amorphous carbon film. To make a contrast, the purified graphite was also heat treated in the same way. The pristine natural graphite, heat-treated purified graphite and RF (resorcinol–formaldehyde) encapsulated powders are coded as NG_{UN}, NG_R and NG_B, respectively, hereafter.

X-ray diffraction (XRD) analysis (D/max-RB diffractometer with Cu Kα radiation.) was used. The Brunauer–Emmet–Teller (BET) surface area was measured with a Quantachrome Autosorb automated gas sorption system using nitrogen gas. Surface disordering of RF encapsulated graphite was investigated by Raman spectrometer (Microscopic Confocal Raman Spectrometer, Renishaw, RM200 with Ar ion laser of 514.5 nm). Secondary

electron microscopy (SEM) and energy dispersive X-ray (EDX) analysis were also used in the analysis of the impurities.

To test the electrochemical performance of the modified graphite, graphite electrode laminates were prepared by casting onto a copper foil a slurry consisting of either the treated or untreated graphite powder (80 wt.%), acetylene black (5%)and poly(vinylidene fluoride) (PVDF) (15 wt.%) dispersed in ethanol. The electrodes were then dried at 120 °C under vacuum for 24 h.

The galvanostatic charge–discharge cycling of the treated or untreated graphite materials was carried out using a coin-type test cell, in which Li metal foil was used as the counter electrode. The electrolyte was 1.0MLiPF6 dissolved in a mixture of ethylene carbonate and diethyl carbonate (1:1, v/v). CR2025-type coin cells were assembled in a glove box (M. Braun GmbH, Germany) with H_2O and O_2 content below 1 ppm. The measurement of the cycling performance of these cells was performed on a multi-channel battery cycler (LAND, WuHan) at a current density of 0.25 mA cm^{-2} in the voltage range between 0.02 and 2 V at room temperature.

3. Results and discussion

Fig. 1 shows the voltage profiles of three half cells using NG_{UN}, NG_R and NG_B as the working electrodes, respectively. It is evident that there are notable differences in these curves; especially of the charge curves, indicating that the initial charge–discharge performance of treated natural graphite in comparison with untreated one has been greatly improved. From the figure, it is clear that the three discharge curves are quite similar in shape. This reflects that the modification does not change general structure of natural graphite. During the first intercalation, an initial dramatic drop is seen from the open circuit voltage to around 0.6 V (versus Li/Li$^+$) and then a single plateau is formed. It is followed that the voltage gradually descends with the lithium intercalation and long plateau appears at the region of 0.25–0 V (versus Li/Li$^+$). The plateau at 0.6 Vand slope at
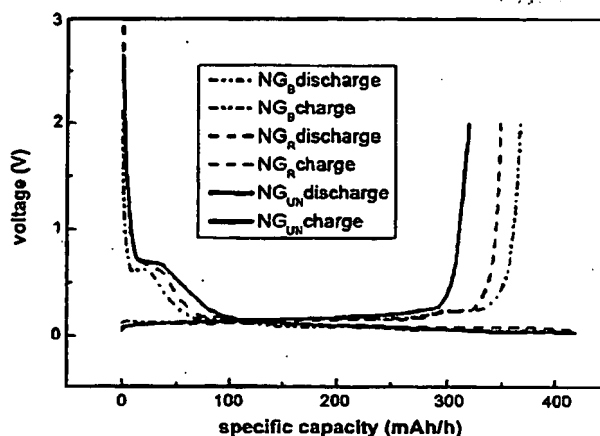

Fig. 1. The initial charge–discharge curves for pristine graphite (NG_{UN}), heat-treated purified graphite (NG_R) and carbon encapsulated graphite (NG_B) at a current density of 0.25 mA cm^{-2}.
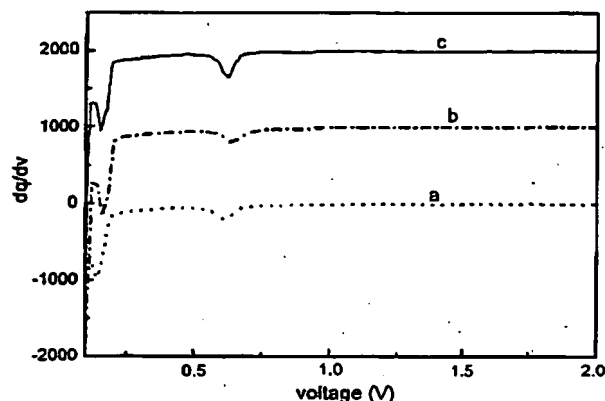
Fig. 2. Differential capacity vs. voltage for first lithium intercalation for (a) carbon encapsulated graphite (NG$_B$), (b) heat-treated purified graphite (NG$_R$) and (c) pristine graphite (NG$_{UN}$).

Fig. 3. The charge–discharge cycling performance curves of pristine graphite (NG$_{UN}$), heat-treated purified graphite (NG$_R$) and carbon encapsulated graphite (NG$_B$).

the region of 0.6–0.25 V (versus Li/Li$^+$) is related to the electrochemical decomposition of the electrolyte and formation of a thin film (SEI) on graphite electrode [19], both of which take place simultaneously on the surfaces of the carbon particles. The purified and carbon-coated samples, especially the carbon-coated one show a comparatively short plateau and slope as compared with that of the pristine graphite sample. The main capacities were released below 0.25 V (versus Li/Li$^+$), i.e. the second plateau (the long one), which is corresponding to the main intercalation processes of lithium in graphite occurring by staging from 0.25 V (versus Li/Li$^+$) to 0 V (versus Li/Li$^+$). The electrolyte decomposition and the formation of the SEI layer are the cause of irreversible capacities.

Fig. 2 shows differential capacity versus voltage for first lithium intercalation of three graphite samples. The irreversible peak near 0.6 V (versus Li/Li$^+$) in Fig. 2 is caused by side reactions, which take place at the edges of the graphite, i.e. a process called "exfoliation". The modified graphite samples, especially the carbon-film-coated one (Fig. 2b) shows a rather smaller peak near 0.6 V (versus Li/Li$^+$) than that of the pristine graphite sample (Fig. 2c). This suggests that the concentration of active edge sites at the surfaces of the graphite sample is reduced significantly by purifying under the condition of high temperature hydrothermal process and coating the graphite with RF resin via in situ polymerization.

Table 1 summarizes the results of the BET surface areas and charge–discharge characteristics of three graphite samples. The first discharge capacities of three graphite electrodes are all more than 400 mAh g^{-1}, exceeding the theoretical capac-
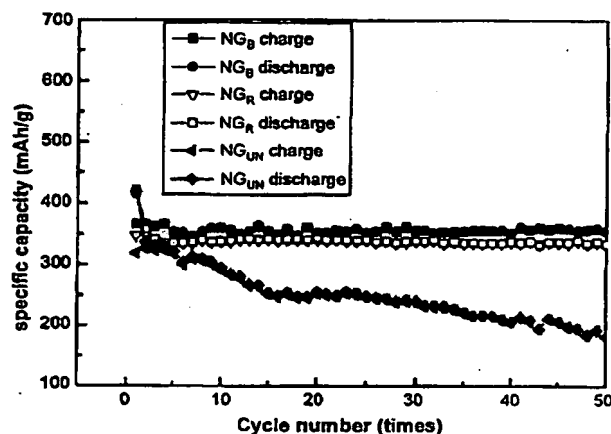
ity (372 mAh g^{-1}) of graphite. The first charge capacities of them increase in turn from NG$_{UN}$ electrode to NG$_B$ electrode, which reaches 366.5 mAh g^{-1}, close to the theoretical capacity of graphite. The first irreversible capacity loss of NG$_{UN}$ electrode is higher than that of NG$_R$ electrode, whereas NG$_B$ electrode has the lowest one (48.4 mAh g^{-1}). Accordingly, the initial coulombic efficiency of NG$_{UN}$ (74.9%) is lower than that of the NG$_R$ electrode (82.7%) and the NG$_B$ electrode (88.4%).

Fig. 3 shows the plot of the charge and discharge capacity as a function of cycle number for three graphite samples, indicating that the reversible capacities of treated graphite electrodes is higher than that of pristine electrode. The cycling performance curve of NG$_R$ electrode presents smooth and stable state after the fourth cycle, though capacities of its foremost cycles show slight drop with the increase of cycle number. NG$_B$ electrode has almost the same cycling performance curve shape as that of NG$_R$ electrode but keeps above the latter one, which indicates the reversible capacity of the former is higher than that of the latter for all cycles. NG$_{UN}$ electrode has considerable difference with NG$_R$ or NG$_B$ electrode in the cycling performance curve shape. Its curve takes on gradual drop trend with cycle numbers, therefore showing bad capacity retention. The reversible capacities of 333.5 and 355.8 mAh g^{-1} after 50 cycles can be retained respectively with the NG$_R$ and NG$_B$ electrode, while the pristine graphite electrode (NG$_{UN}$) retained only 180.7 mAh g^{-1}. Consequently, the capacity retentions of the three graphite electrodes after 50 cycles are 97%, 96% and 56.7%, respectively. The small rise in the reversible capacity after the sixth cycle for

Table 1

Charge–discharge characteristics of the pristine graphite, heat-treated purified graphite and coated purified graphite after heat-treatment

Sample	First discharge capacity (mAh g^{-1})	First charge capacity (mAh g^{-1})	Initial irreversible capacity (mAh g^{-1})	Initial charge–discharge efficiency (%)
NG$_{UN}$	418	318.5	99.5	76.2
NG$_R$	420.6	347.9	72.7	82.7
NG$_B$	414.9	366.5	48.4	88.4

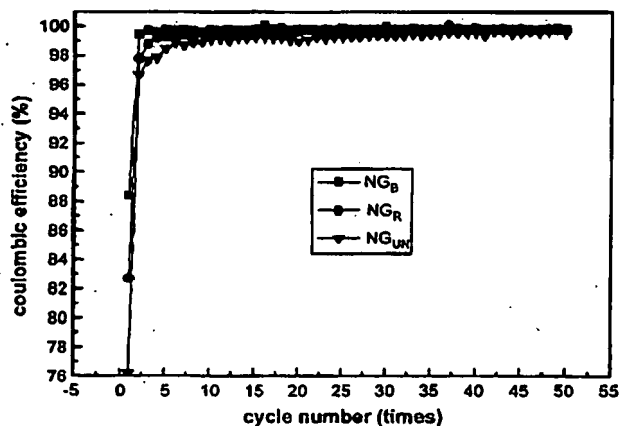Fig. 4. Coulombic efficiency of pristine graphite (NG$_{UN}$), heat-treated purified graphite (NG$_R$) and carbon encapsulated graphite (NG$_B$).
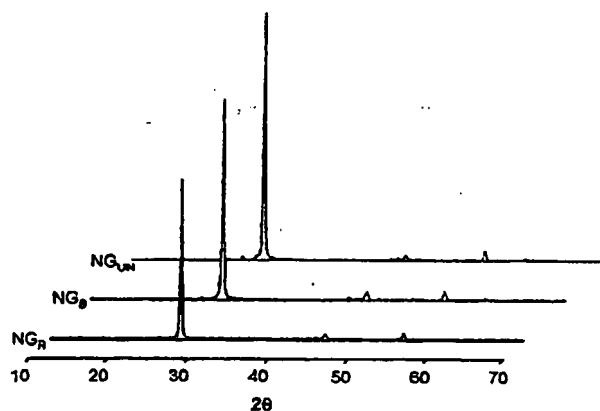

Fig. 5. XRD patterns of three graphite powders: (1) heat-treated purified graphite (NG$_R$), (2) carbon encapsulated graphite (NG$_B$) and (3) pristine graphite (NG$_{UN}$).

the NG$_{UN}$/Li cell is possibly due to impurity effect. For NG$_R$, the impurity could be eliminated so that it does not cause such a capacity change.

Fig. 4 shows the coulombic efficiency of NG$_B$ NG$_R$ and NG$_{UN}$ in 50 cycles. NG$_B$ electrode not only presents the highest initial coulombic efficiency, but also almost keeps constant value after two cycles. In contrast, the coulombic efficiency of NG$_R$ electrode is not as good as that of NG$_B$, whereas NG$_{UN}$ is the worst one. It both exhibits the lowest initial coulombic efficiency and the lowest one for the latter cycles. This is why pristine graphite has the worst cycling performance.

Fig. 5 shows the X-ray diffraction patterns of the graphite powders NG$_{UN}$, NG$_B$ and NG$_R$, indicating that all of the three

patterns show almost the same diffraction peaks of graphite crystals. This once again exhibits that the modifying process of purification or encapsulation on graphite does not damage its essential structure, which is favorite one in the anode for lithium ion batteries. In addition, it can be noted that in the case of carbon encapsulated graphite, no broadening diffraction peaks of amorphous carbon are found. It is well known that, when the thickness of film, especially that of amorphous carbon film, is too thin, the diffraction peaks of the film will not be presented effectively in XRD patterns. However, the status of carbon film coated on the graphite particles can be clearly observed by means of SEM images of carbon encapsulated graphite. Otherwise, it can be also noticed that the diffraction peak
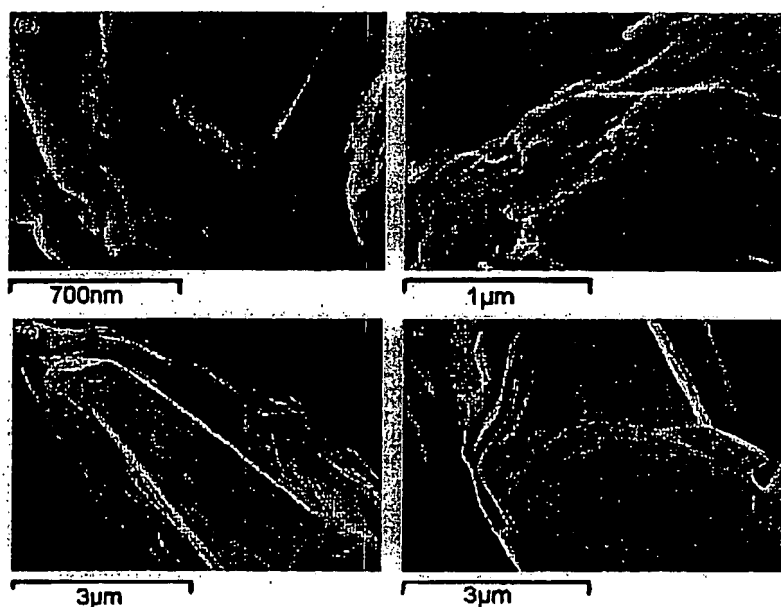

Fig. 6. SEM images of graphite samples: (a and b) carbon encapsulated graphite (NG$_B$), (c) the pristine graphite and (d) heat-treated purified graphite (NG$_R$).

strength of untreated graphite is somewhat stronger than those of the others, which seems to indicate that modified graphite materials improve the disordered structures of the surface region of carbon materials and thus affect their diffraction peak strength.

Fig. 6 shows the scanning electron microscope (SEM) images of the three graphite samples. Fig. 6a and b shows the images of carbon encapsulated graphite. From the images, it can be obviously observed that there is a film layer coating on the surface of graphite while no film layer appears in the SEM images of pristine natural graphite (Fig. 6c) and heat-treated purified graphite (Fig. 6d). Obviously, it can be considered that the film layer comes from pyrolyzed RF resin coated on natural graphite particles. Moreover, the film layer is so thin that it both seems transparent and no micropores and/or nano-channels on it. Furthermore, owing to in situ encapsulated graphite process via interfacial polymerization, it can be seen that the film layer coated on natural graphite particle is very complete and homogeneous. Fig. 6c is the SEM image of NG$_{UN}$, from which the surface structure containing a lot of sharp edges and fragments can be observed, while at the SEM images of NG$_R$ (Fig. 6d), NG$_B$ (Fig. 6 a and b), the sharp edges and fragments of the graphite particles are not as obvious as in NG$_{UN}$. Obviously, after purifying and coating treatment, the surface defects of natural graphite such as sharp edges and fragments are 'repaired', which is beneficial to the improvement of the electrochemical performance of the natural graphite. From EDS (energy dispersive spectrometer) plots and component analysis of three graphite samples, almost no difference can be observed, in addition to slight distinctness in oxygen content. The increases of oxygen content in heat-treated purified graphite (NG$_R$) and carbon encapsulated graphite (NG$_B$) are probably related to the passivating film formed on their surfaces.

Fig. 7 shows the Raman spectrum of three graphite sample. Raman spectroscopy distinguishes ordered and disordered structures of the surface region of carbon materials. A band observed at 1581 cm^{-1} arises from an E_{2g} vibration mode in
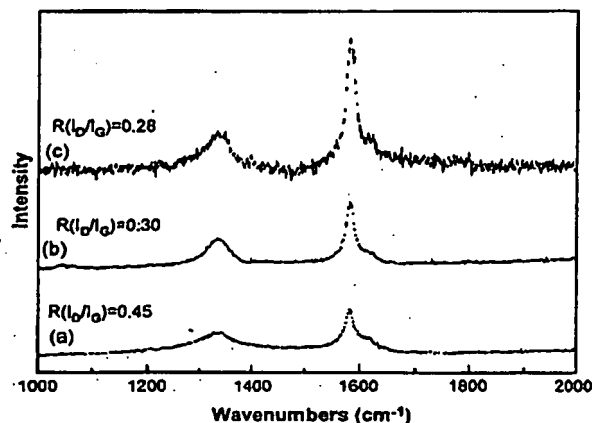
the graphitic region of carbon materials (G-band) while another band at 1339 cm^{-1} is due to an A_{1g} mode in the disordered region of carbon materials or edge plane of powdery carbon (D-band) [20]. The ratio of intensity ($R = I_D/I_G$) of D-band to that of G-band well exhibits the degree of disordering of surface area of carbon materials. The peak positions of Raman bands are not modified by purification or encapsulation on natural graphite but the notable increase in the peak intensity and breadth as in the case of treated graphite, especially encapsulated graphite, indicating the increase in the surface disordering and the presence of amorphous carbon film.

4. Conclusions

After the purified graphite is gained by treating natural graphite in high temperature hydrothermal autoclave under the condition of concentrated hydrochloric acid and concentrated sulfuric acid, a RF-coated graphite powder can be prepared via resorcinol–formaldehyde polymerized in situ on the surface of the purified graphite. By means of heat-treatment, coated layer can be converted into amorphous carbon film enclosed graphite. The surface defects and impurities on natural graphite can be eliminated by the purification. The electrochemical performance of heat-treated purified natural graphite shows greatly improved electrochemical performance. The carbon-film encapsulation can further modify its surface structure. Therefore, this study demonstrates that the natural graphite sample coated a thin carbon film presents good initial charge–discharge coulombic efficiency and cycling performance. This approach shows that the material prepared by the proposed process can become a promising anode material with excellent performance price ratio for rechargeable lithium batteries.

Acknowledgements

Fig. 7. Raman spectra of (a) carbon encapsulated graphite (NG$_B$), (b) heat-treated purified graphite (NG$_R$) and (c) pristine graphite (NG$_{UN}$).

References

[1] J. Shim, K.A. Striebel, J. Power Sources 119–121 (2003) 955.

[2] Y.P. Wu, C. Jiang, C. Wan, R. Holze, Solid State Ionics 156 (2003) 283.

[3] Y.P. Wu, E. Rahm, R. Holze, J. Power Sources 114 (2003) 228.

[4] J.J. Li, X.M. He, C.Y. Jiang, C.R. Wan, J. New Mater. Electrochem. Syst. 9 (2006) 21.

[5] M. Yoshio, H. Wang, K. Fukuda, Y. Hara, Y. Adachi, J. Electrochem. Soc. 147 (2000) 1245.

[6] K. Guerin, F.B. Annie, S. Flandrois, J. Electrochem. Soc. 146 (10) (1999) 3360.

[7] Y.P. Wu, C.R. Wan, C.Y. Jiang, J.J. Li, Y.X. Li, Chinese Chem. Lett. 10 (1999) 339.

[8] K. Zaghib, X. Song, A. Guerfi, R. Rioux, K. Kinoshita, J. Power Sources 119–121 (2003) 8.

[9] J.P. Olivier, M. Winter, J. Power Source 151–155 (2001) 151.

[10] K.K. Guo, Q.M. Pan, S.B. Fan, J. Power Sources 111 (2002) 350.

[11] M. Yoshio, H. Wang, K. Fukuda, T. Umeno, T. Abe, Z. Ogumi, J. Mater. Chem. 14 (2004) 1754.

[12] M. Yoshio, H. Wang, K. Fukuda, Angew. Chem. Int. Ed. 42 (2003) 4203.

[13] Z.H. Yu, F. Wu, Battery Bimonthly 33 (2003) 131 (in Chinese).

[14] Q.M. Pan, K.K. Guo, L.Z. Wang, S.B. Fang, Solid State Ionics 149 (2002) 193–200.

[15] E. Peled, C. Menachem, A. Melman, J. Electrochem. Soc. 143 (1996) L4.

[16] Y.P. Wu, C. Jiang, C. Wan, J. Li, Chinese J. Batteries 30 (2000) 143.

[17] H. Buqu, P. Golob, M. Winter, J.O. Besenhard, J. Power Sources 97/98 (2001) 122.

[19] N. Tsuyoshi, G. Vinny, O. Yoshimi, I. Hiroyuki, J. Fluorine Chem. 114 (2002) 209–221.

[20] T. Nakajima, V. Gupta, Y. Oheawa, M. Koh, R.N. Singh, A. Tressaud, E. Durand, J. Power Sources 104 (2002) 108–114.